STRATOSPHERIC INFLUENCE ON THE BREAKDOWN OF A JANUARY 2009 BLOCKING EPISODE

A Thesis

Presented to the Faculty of the Graduate School

of Cornell University

in Partial Fulfillment of the Requirements for the Degree of

Master of Science

by

Michael Ewens Kelleher

May 2010

ABSTRACT

In previous research on atmospheric blocking the interest has primarily been on the onset of blocking. To fully understand a blocking episode, the end, or breakdown, must also be investigated. The focus of this research was to examine the dynamics of block breakdown, with special notice to the stratospheric influence. Several factors that have been previously discussed in block onset, including advection of quasi-geostrophic potential vorticity, temperature advection, and adiabatic temperature changes, were examined both at block breakdown and block onset for comparison. The calculations were done on Weather Research and Forecasting (WRF) model runs. The WRF was initialized with three different types of initial and boundary conditions from the blocking episode on 10-20 January 2009: a Global Forecast System (GFS) Final Analysis, GFS real-time 180 hour forecast, and modified GFS real-time 180 hour forecast. To perform the runs based on modified GFS forecasts, several temperature modifications were made in both the stratosphere and lower troposphere on both onset and breakdown runs of the WRF. The impact of the modifications were observed to be the greatest magnitude at block breakdown. Cooling the stratosphere had the effect of sustaining the block for up to 12 hours, and up to 24 hours longer when the troposphere was warmed. The modification at block onset did not change the timing significantly but did impact the strength. In the future, this technique will be applied to other case studies so that the results may be corroborated, as one case study does not indicate a more general pattern.

BIOGRAPHICAL SKETCH

Michael Ewens Kelleher was born near the shore of Lake Ontario in Oswego, New York to William and Carolyn Kelleher. He attended school in the Oswego City School district and graduated from Oswego High School. During his school career, he was an active member of the Boy Scouts of America, ultimately achieving the rank of Eagle Scout. Upon graduation from high school, he attended SUNY Oswego, earning undergraduate degrees in in Meteorology and Applied Mathematics. While at SUNY Oswego, he participated in the Oswego State Student Chapter of the AMS. This included becoming Treasurer and Vice President as well as serving on the committee of the first and second annual Lake Effect Conference (now called Great Lakes Atmospheric Science Symposium). Michael is also a student member of Sigma Xi, the Scientific Research Society. In his senior year at SUNY Oswego, he had the opportunity to do research with Dr. Steven Skubis on large scale and wave dynamics. It was this research that ultimately led him to Cornell University to work with Dr. Stephen Colucci, where he has been for nearly two years.

To my family, Mom, Dad and Sally, you have made me what I am today. Your support and encouragement made this possible.

Go raibh míle maith agaibh!!

ACKNOWLEDGEMENTS

I would like to acknowledge the invaluable guidance of my advisor Dr. Stephen Colucci, whose weekly meetings formed the ideas for this research, and kept me on track and down to Earth. I would also like to acknowledge the guidance from my special committee members Drs. Gang Chen and Leonard Gross.

I would also like to acknowledge the support of my fellow graduate students Steve Jessup, Christina Patricola, Rachel Scanza and Marcus Walter for their friendship and for help along the way. Also, Brian Belcher for providing technical assistance including providing the code for the modification programs. In addition, I would like to acknowledge Pam Vitale for her assitance.

The GFS Final Analysis data for this study are from the Research Data Archive (RDA) which is maintained by the Computational and Information Systems Laboratory (CISL) at the National Center for Atmospheric Research (NCAR). NCAR is sponsored by the National Science Foundation (NSF). The original data are available from the RDA (http://dss.ucar.edu) in dataset number ds083.2.

The GFS real-time data for this study are from the National Operational Model Archive and Distribution System (NOMADS).

TABLE OF CONTENTS

LIST OF TABLES

LIST OF FIGURES

CHAPTER 1

INTRODUCTION

Atmospheric blocking refers to a large scale high pressure system that interrupts the typical zonal (West to East) flow in the mid-latitudes. The high pressure, or ridge, diverts low pressure systems (called cyclones or troughs) around a large area. To be considered a block, this pattern must persist for five or more days in the same area.

Blocking research has, for the most part, been focused on block onset and maintenance and several factors have been studied. The breakdown of blocking has not been studied as extensively, though the Cash and Lee (2000) study focused on the entire evolution, including the decay or breakdown.

The blocking problem is not just simply an interesting academic problem as it has a real impact on weather over large areas for many days. Carrera et al. (2004) found that a typical Alaskan block could affect temperatures from the Yukon in Canada to the Great Plains in the US and Trenberth and Guillemot (1996) found a relationship to droughts and floods. Forecasting a block can be critical to a forecast for anywhere from a few days to seven or more.

Previous diagnostic and observational studies have investigated a number of factors involved in block onset, including diffluent flow preconditioning (Colucci, 2001), interactions between Potential Vorticity (PV) and deformation Dong and Colucci (2007) and a non-linear self-interaction of vorticity (Cash and Lee, 2000). Colucci and Alberta (1996) also found a relationship between strong southerly winds over a cyclone coupled with weak planetary scale westerlies as a precursor to blocking. A relationship to diabatic heating in the Southern Hemisphere was found by Tilly et al. (2008) but was determined to have less of an effect than vorticity advection.

Tropospheric influence on tropospheric weather systems has long been known, as has an intraseasonal influence of the stratosphere on tropospheric systems. Garfinkel et al. (2010) notes an effect of tropospheric systems weakening stratospheric vorticies. It is only in a few studies, including Colucci (2010), that note a stratospheric influence on synoptic temporal and spacial scale weather systems. Synoptic scale systems are those systems that last for days to a week that span thousands of kilometers.

In this paper, a case study will be discussed with concentration on stratospheric effects on the block evolution. Multiple Weather Research and Forecasting (WRF) model runs were performed with both final analysis and real-time boundary conditions. To investigate the effects of temperature on block evolution, the real-time boundary conditions were modified to produce different results. First, a discussion will take place on the various theoretical frameworks used to investigate the event, then the specific methods used will be discussed, finally several of the various model runs of the blocking event will be discussed.

CHAPTER 2

THEORETICAL FRAMEWORK

2.1 Quasigeostrophic Theory

The basis of quasigeostrophic theory is the quasigeostrophic approximation, where horizontal winds are replaced with the geostrophic wind in the acceleration terms of the momentum equations and horizontal advection becomes geostrophic advection in the thermodynamic equation. The static stability parameter, which varies in space and time, is replaced with a static stability parameter which varies only with height. Finally, vertical advection of momentum is neglected, according to Holton (2004).

This simplifies the equations of momentum and thermodynamics to a level which, on the synoptic scale, facilitates quicker and simpler calculations without loss of significant precision. This works well for blocking research, as it is a large system in both spacial and temporal resolution.

2.2 Quasigeostrophic potential vorticity

Quasigeostrophic potential vorticity (QGPV) has been used in the past as a diagnostic tool for large scale systems, including blocking. In Dong and Colucci (2007) QGPV and the advection of it were examined as important tools in block diagnosis. QGPV is defined as follows

$$q = \frac{g}{f_0}\nabla^2 z + f + f_0 g \frac{\partial}{\partial p}\left[\frac{1}{\sigma}\frac{\partial z}{\partial p}\right] \tag{2.1}$$

where z is geopotential height, g is acceleration due to gravity, f_0 is the Coriolis parameter at 45°latitude, f is the Coriolis parameter at a given latitude, and σ is the static stability parameter $\sigma = -\frac{\alpha}{\theta}\frac{\partial\theta}{\partial p}$, for potential temperature, θ (see appendix equation B.1), specific volume α and pressure p.

2.3 Height tendency

To analyze the factors involved in height change, the quasigeostrophic assumptions are used to develop an equation for height tendency, $\chi = \frac{dz}{dt}$, where z is height, that can be split into components. The adiabatic quasigeostrophic height tendency equation is

$$\left[\nabla_p^2 - \frac{f_0^2}{\sigma}\frac{\partial\sigma}{\partial p}\frac{\partial}{\partial p} + \frac{f_0^2}{\sigma}\frac{\partial^2}{\partial p^2}\right]\chi = -\frac{f_0}{g}\vec{V}_g \cdot \nabla_p\left(\zeta_g + f\right) + \frac{f_0^2 R_d}{g}\frac{\partial}{\partial p}\left[\frac{\vec{V}_g \cdot \nabla_p T}{\sigma p}\right] \tag{2.2}$$

With χ_v being mechanically or vorticity forced height change, and χ_T being thermally forced height change, the parts of equation (2.2)

$$F_V = \frac{-g}{f_0}\left(\vec{V}_g \cdot \nabla\left(\zeta_g + f\right)\right) \tag{2.3}$$

$$F_T = \frac{-R_d f_0^2}{g}\frac{\partial}{\partial p}\left[\frac{\vec{V}_g \cdot \nabla_p T}{\sigma p}\right] \tag{2.4}$$

are the forcing functions for each. Here

$$\vec{V}_g = \frac{g}{f_0}\left(-\frac{\partial z}{\partial y}\hat{\imath} + \frac{\partial z}{\partial x}\hat{\jmath}\right) \tag{2.5}$$

is the geostrophic wind, $\zeta_g = \frac{\partial v_g}{\partial x} - \frac{\partial u_g}{\partial y}$ is the geostrophic relative vorticity, $R_d = 287 K^{-1} m^2 s^{-2}$ is the dry gas constant and T is temperature. To solve these for the height change, a successive-over-relaxation method is used, where a residual is calculated from the forcing function, F_T for χ_T and F_V for χ_V.

2.4 Vertical integrals of temperature change

To see the height change on a particular level as a function of multiple levels above it, a diagnostic model following Colucci (2010) was used. Starting with hydrostatic balance

$$\frac{\partial z}{\partial p} = -\rho g = -\frac{R_d T}{pg} \tag{2.6}$$

replacing density by way of the ideal gas law $p = \rho R_d T$, differentiating with respect to time t, and substituting the Eulerian thermodynamic energy equation for temperature change, the following is obtained after integrating between two pressure levels P_b and P_t for the bottom and top levels respectively.

$$\frac{\partial z_b}{\partial t} = \frac{\partial z_t}{\partial t} - \frac{R_d}{g}\int_{p_t}^{p_b}\left(\frac{J}{c_p} - \vec{V_H}\cdot\nabla_p T + \frac{\omega\sigma p}{R_d}\right)\frac{dp}{p} \tag{2.7}$$

Here ω is the vertical motion with respect to pressure in Pa/s, c_p is the specific heat of dry air at constant pressure in $Jkg^{-1}K^{-1}$, $\vec{V_H}$ is the horizontal wind and J is the diabatic heating rate. This equation relates height change at a lower pressure level to height change at a higher pressure level and thermal processes integrated through the atmosphere. The thermal processes are separated inside the integral into diabatic, advective and adiabatic processes respectively. For this research, the integral was taken for $p_t = 20hPa$ and $p_b = 1000hPa$ to get the height tendency at 500 hPa. It was then separated into tropospheric and stratospheric components to get

$$\left(\frac{\partial z}{\partial t}\right)_{500hPa} = \left(\frac{\partial z}{\partial t}\right)_{1000hPa} + \frac{R_d}{g}\int_{500hPa}^{1000hPa}\left(\frac{J}{c_p} - \vec{V_H}\cdot\nabla_p T + \frac{\omega\sigma p}{R_d}\right)\frac{dp}{p} \tag{2.8}$$

$$\left(\frac{\partial z}{\partial t}\right)_{500hPa} = \left(\frac{\partial z}{\partial t}\right)_{20hPa} - \frac{R_d}{g}\int_{20hPa}^{500hPa}\left(\frac{J}{c_p} - \vec{V_H}\cdot\nabla_p T + \frac{\omega\sigma p}{R_d}\right)\frac{dp}{p} \tag{2.9}$$

Averaging (2.8) and (2.9), 500 hPa height tendency is obtained as a function of lower tropospheric effects, and upper tropospheric and stratospheric effects:

$$\left(\frac{\partial z}{\partial t}\right)_{500hPa} = \left(\frac{1}{2}\right)\left(\frac{\partial z}{\partial t}\right)_{1000hPa} + \frac{R_d}{2g}\int_{500hPa}^{1000hPa}\left(\frac{J}{c_p} - \vec{V_H}\cdot\nabla_p T + \frac{\omega\sigma p}{R_d}\right)\frac{dp}{p}$$

$$+\left(\frac{1}{2}\right)\left(\frac{\partial z}{\partial t}\right)_{20hPa} - \frac{R_d}{2g}\int_{20hPa}^{500hPa}\left(\frac{J}{c_p} - \vec{V_H}\cdot\nabla_p T + \frac{\omega\sigma p}{R_d}\right)\frac{dp}{p} \quad (2.10)$$

Then the upper part of (2.10) is split into tropospheric and stratospheric components to get

$$\left(\frac{\partial z_{500hPa}}{\partial t}\right)_{upper} = \left(\frac{1}{2}\right)\left(\frac{\partial z}{\partial t}\right)_{20hPa}$$

$$-\frac{R_d}{2g}\int_{200hPa}^{500hPa}\left(\frac{J}{c_p} - \vec{V_H}\cdot\nabla_p T + \frac{\omega\sigma p}{R_d}\right)\frac{dp}{p} \quad (2.11)$$

$$-\frac{R_d}{2g}\int_{20hPa}^{200hPa}\left(\frac{J}{c_p} - \vec{V_H}\cdot\nabla_p T + \frac{\omega\sigma p}{R_d}\right)\frac{dp}{p} \quad (2.12)$$

where (2.11) is the contribution from the upper troposphere and (2.12) is the contribution from the stratosphere.

As described in Colucci (2010) the minus sign in front of (2.11) and (2.12) indicate that for diabatic, advective and adiabatic warming in the upper troposphere and stratosphere, 500 hPa height falls result, whereas for cooling, 500 hPa height rises result. This is the opposite result of the lower troposphere where warming results in height rises, and cooling results in height falls.

These parameters were examined both on a horizontal surface plot and as an average over time. The average was taken, as in Colucci (2010) over a 10°x10°area over the fastest height change over each 12 hour time period.

The hypothesis is that warming in the stratosphere results in 500 hPa height falls, and cooling in the stratosphere results in height rises. In this case, the 500 hPa heights are associated with a block, thus rising or falling heights represent a strengthening or weakening block respectively. To test this, a series of experiments was conducted to examine the effects of stratospheric warming and cooling on the onset and breakdown of a particular block. The theory was that stratospheric warming at onset would delay or weaken onset, cooling at onset would enhance or quicken onset, warming at breakdown would accelerate breakdown, and that cooling at breakdown would delay breakdown.

CHAPTER 3

METHODOLOGY AND DATA

3.1 Weather Research and Forecasting Model

The Weather Research and Forecasting (WRF) model was developed by several cooperating institutions including the National Center for Atmospheric Research (NCAR), the National Oceanic and Atmospheric Administration (NOAA), the National Centers for Environmental Prediction (NCEP), the Forecast Systems Laboratory (FSL), the Air Force Weather Agency (AFWA), the Naval Research Laboratory, the University of Oklahoma, and the Federal Aviation Administration (FAA) according to the WRF website (UCAR, 2010). For this research, version 3.1.1 of the Advanced Research WRF (ARW) core of the WRF was used as it is freely available online. No changes were made to the default set of physics or dynamics parameters, except to allow the model domain to run into the stratosphere.

3.2 Input Data

Input data used as initial and boundary conditions were 1.0°x1.0° Global Forecast System (GFS) data. This data fell into three categories: Final Analysis (FNL), real-time unmodified and real-time modified. The real-time data obtained from the National Operational Model Archive and Distribution System (NOMADS) is identical to the data that would be available operationally. The final analysis data was obtained from the NCAR Research Data Archive (RDA),

and is generated from the four daily GFS runs by NCEP. This data was used as a best-possible case boundary and initial conditions as it is the closest possible data to actual conditions.

To initialize the WRF with GFS data, five preprocessor programs are run. A preprocessor for the geographic data is standard for all WRF runs. This takes raw geographic input data and defines a new file for each domain that the WRF is to use. Then the data from the GFS, in Gridded Binary (GRIB) format, is put into a temporary format that is then read by a utility to interpolate the GFS data to pressure levels, including the stratosphere. The final preprocessor program, metgrid, combines the geographic data with the meteorological data by interpolating the intermediate format to the model domain horizontally into NetCDF format. Finally, the data is interpolated to vertical levels by the real data initialization program before the WRF model run is initialized. The WRF model was run at a 95km grid spacing with 145 x-axis data points, 120 y-axis data points, 28 vertical levels, and a temporal resolution of 3 hours.

3.3 Modification of Boundary Conditions

To produce the modified boundary conditions, the metgrid data is used as input to a Python program that uses the NetCDF library to modify the chosen variables, in this case, temperature. To smoothly modify temperature, the mean and standard deviation were taken for the entire level, then the following equation was applied.

$$T(x, y, p, t) = T(x, y, p, t) + \frac{n}{\sigma} * |T - \mu| \tag{3.1}$$

Where μ and σ are the mean and standard deviation for the pressure level p respectively and n is an integer multiplier with $1 \leq |n| \leq 8$. This multiplier was

necessarily less than 8 as it was found that a multiplier greater than 8 for almost all cases caused the WRF model run to fail to complete.

To select the area to be modified, five different methods were utilized. The simplest was to modify the entire domain of the model run, either warming or cooling the whole domain. Next was a selected warm or cool area, simply warmer or cooler than the mean for that level. It was also possible to selectively warm an area based on the height at 500 hPa at each time.

The final two methods were to select a polygon to modify. First, an area around just the block was used, with a 15°x 15°area centered on the largest absolute value of height change at the particular time. These were the most delicate of modifications, with $|n| < 5$. For anything greater than 5, the model run failed to complete. It is hypothesized that at this point numerical instability developed as the new initial conditions were too far from what would occur in the real atmosphere.

3.4 Data Analysis

To analyze the data produced by WRF model runs, a library of NCAR Command Language (NCL) scripts were developed in concert with a library of Fortran functions to be called from within the NCL scripts. Each NCL script took in raw data from the WRF, performed interpolation to pressure levels (e.g. 500 hPa, 20 hPa) then performed calculations on the interpolated data and finally output a graphical representation. A list of Fortran functions is available in Appendix A.

CHAPTER 4

CASE STUDY

4.1 Overview of January 2009

For the case considered in this study, an approximation of Watson and Colucci (2002) definition of a block was used, that is, a negative zonal index (500 hPa heights higher at 60°N than at 40°N over 20°longitude) persisting for five or more days. This was approximated by shifting the strict latitude definition. The block onset occurred at 1200Z on 10 January 2009 (*fig. 4.1(a)*), and decay or breakdown occurred between 0600Z and 1200Z on 20 January 2009 (*fig. 4.1(d)*), giving the block a 10 day lifespan. The stratosphere was characterized by a northerly temperature gradient (temperature decreasing northward) before onset. During the lifespan of the block, the stratospheric gradient shifted to easterly with the cold pool at 20 hPa to the east of the ridge and a warm pool to the west. During the decay, the 20 hPa thermal gradient reversed to a southerly direction.

The block was examined in terms of QGPV and QGPV advection, and height tendency separated into mechanically and thermally forced terms. In this way, the block fit previous theory well. QGPV was dominated by the planetary vorticity. At onset, QGPV advection was anticyclonic near the center of the block and during the block lifespan was cyclonic to the west and anticyclonic to the east, with very little occurring within the block as seen in *fig. 4.2*. Near the decay of the block, cyclonic QGPV advection is noted near the center of the block.

The mechanically forced height tendency dominates slightly over the thermally forced term and both exhibit similar patterns of positive height tendency

to the east and negative to the west, seen in *figure 4.3*.

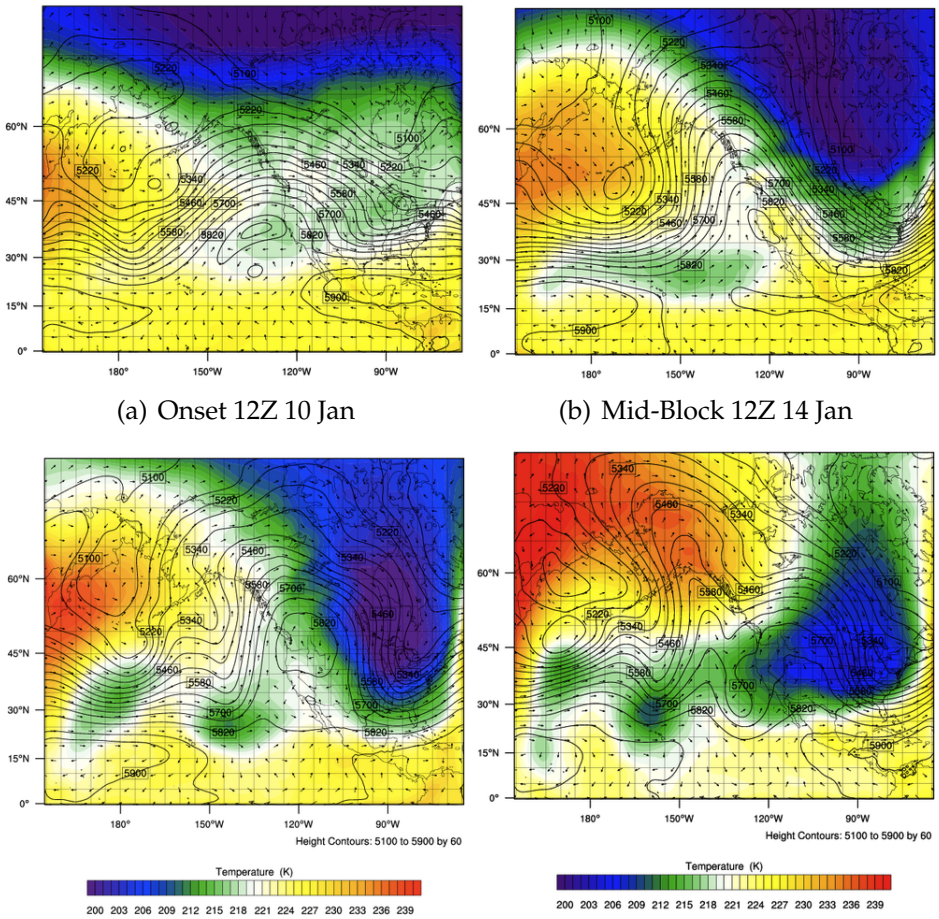

(a) Onset 12Z 10 Jan

(b) Mid-Block 12Z 14 Jan

(c) Mid-Block 00Z 19 Jan

(d) Breakdown 12Z 20 Jan

Figure 4.1: Block evolution: Contoured 500 hPa height (m), colored 20 hPa temperature(K)

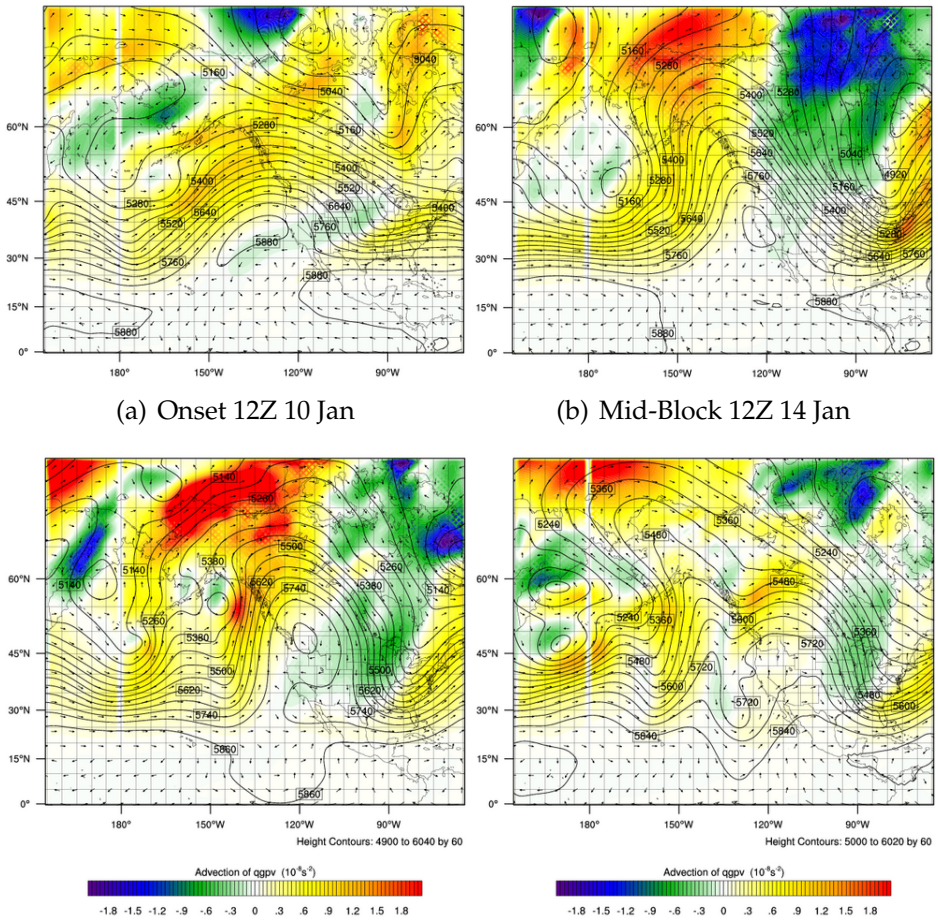

(a) Onset 12Z 10 Jan

(b) Mid-Block 12Z 14 Jan

(c) Mid-Block 00Z 19 Jan

(d) Breakdown 12Z 20 Jan

Figure 4.2: Block evolution: Contoured 500 hPa height (m), colored 500 hPa QGPV advection ($10^{-8}s^{-2}$)

4.2 Unmodified boundary conditions

4.2.1 Onset

The first model runs tested were the real-time unmodified boundary conditions, with the first of these being a model run initialized at 0000Z 08 January 2009. This produced a qualitatively good forecast for the block onset. As illus-

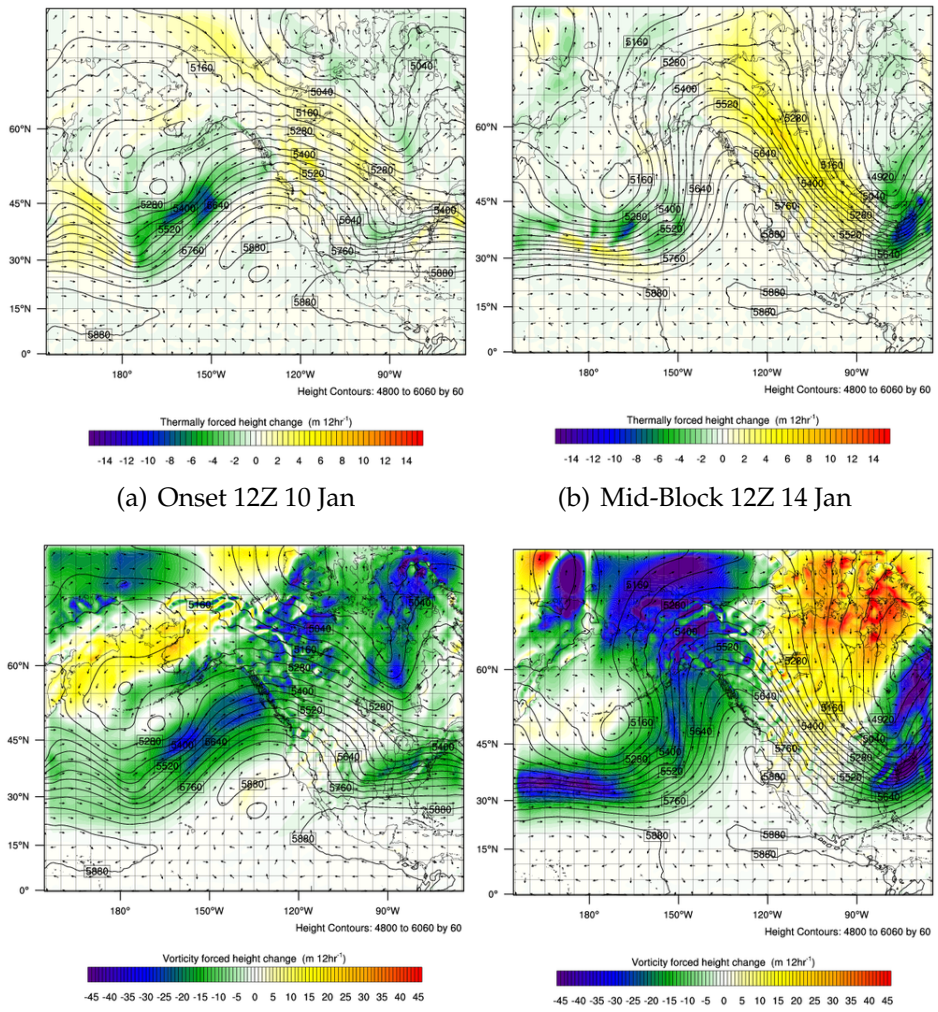

(a) Onset 12Z 10 Jan (b) Mid-Block 12Z 14 Jan

(c) Onset 12Z 10 Jan (d) Mid-Block 12Z 14 Jan

Figure 4.3: Height Tendency at selected times. Contoured 500 hPa height(m), shaded 500 hPa χ_T (a) and (b), χ_V (c) and (d) $(m12hr^{-1})$

trated in *figure 4.4*, both timing and location of onset are nearly identical to the final analysis.

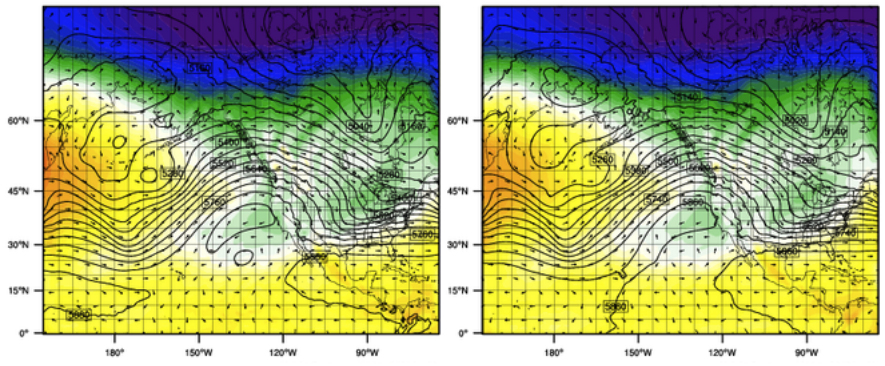

Figure 4.4: Shaded 20hPa temperature (K), contoured 500hPa height (m) at 12Z 10 Jan 2009. FNL on left, Real-time forecast on right.

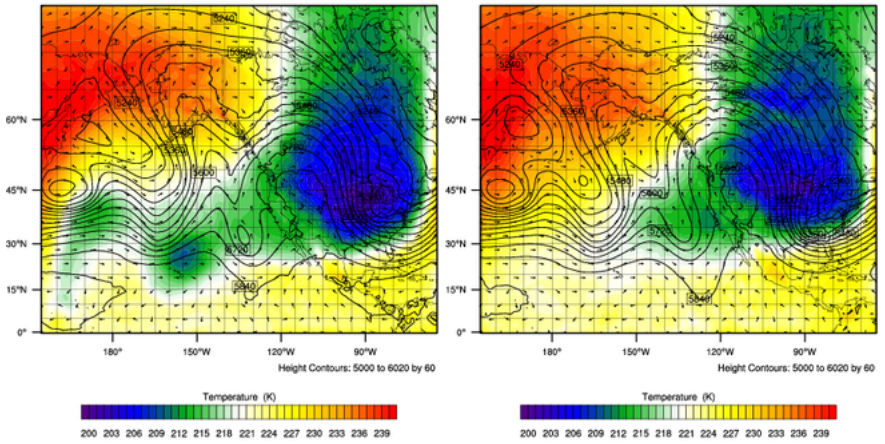

Figure 4.5: Shaded 20hPa temperature (K), contoured 500hPa height (m) at 12Z 20 Jan 2009. FNL on left, Real-time forecast on right.

4.2.2 Breakdown

The second unmodified run was initialized at 0000Z 19 January 2009, 36 hours before breakdown. This run also produced a qualitatively good forecast of timing and intensity of the block. *Figure 4.5* shows the 500 hPa height and 20 hPa temperature for 1200Z 20 January 2009 in the same configuration as *fig. 4.4*. However, a slight difference is noticed between the final analysis based forecast

and the real-time forecast in the 20 hPa temperature field. While the 500 hPa heights on this run were very similar, the real-time forecast was for a slightly stronger block just before breakdown, in the area where 20 hPa temperatures were cooler.

CHAPTER 5

MODIFIED BOUNDARY CONDITIONS

The second set of model runs undertaken were those with modified boundary conditions. As mentioned above, the temperature was modified in specific ways for each the onset and breakdown. Tables 5.1 and 5.2 contain a list of the modified boundary condition WRF runs that were performed and a brief description of what modification took place, where $T = T(x, y, p, t)$, $\sigma_p = \sigma_p(t)$ is the standard deviation of the temperature on pressure level p at time t, $\mu_p = \mu_p(t)$ is the mean of the temperature on pressure level p at time t, $\sigma_Z = \sigma_Z(t)$ is the standard deviation of the 500 hPa height at time t, and $\mu_Z = \mu_Z(t)$ is the mean of the 500 hPa height at time t. In these cases, following the Colucci (2010) definition, the stratosphere is defined to be $p \leqslant 200hPa$ and the lower troposphere defined to be $950hPa \leqslant p \leqslant 550hPa$. In this section several of the more interesting model runs will be discussed, with both intuitive and counter-intuitive results.

5.1 Onset

5.1.1 Warming cool area

The first of the modified runs that will be inspected will be the warming of cool areas at onset, one of the simplest modifications. The predicted outcome of this experiment was to reduce adiabatic and advective cooling, resulting in a weaker block or a delayed onset. As seen in *fig. 5.1*, the modification produced a block at onset time, but the block was weakened, that is that heights were too low in the blocking ridge.

Table 5.1: Warming modifications

Warm All	Whole stratosphere was warmed by 10K.
Warm cool area	Warmed cool areas of the stratosphere (defined by $T < \mu_p$) by *eqn. 3.1* with $n = 8$
Warm by height	Warmed areas of the stratosphere above the 500 hPa ridge ($Z(500hPa) > 5700m$) by $$T = T + \frac{5}{\sigma_p} \cdot |T - \mu_p| \cdot \frac{5 * \sigma_Z}{|Z - \mu_Z|} \quad (5.1)$$
Warm inside ridge	Warmed areas of the stratosphere by selecting a polygon around the block, and when (x,y) is in the polygon, $$T = T + \frac{8\sigma_Z}{|Z - \mu_Z| \cdot \sigma_p} \cdot |T - \mu_p| \quad (5.2)$$
Warm all lower troposphere	Warmed entire lower troposphere by 10K.
Warm troposphere by height	Warmed areas of the lower troposphere by *eqn. 5.1*
Warm troposphere inside ridge	Warmed areas of the lower troposphere by *eqn 5.2*
Warm height change	Warmed 15°x 15°area of stratosphere above the fastest 12-hour 500 hPa height change by *eqn. 3.1* with $n = 5$.

Table 5.2: Cooling Modifications

Cool All	Whole stratosphere was cooled by 10K
Cool warm area	Cooled "warm areas" of the stratosphere (defined by $T > \mu_p$) by *eqn. 3.1* with $n = -8$
Cool by height	Cooled areas of the stratosphere above the 500 hPa ridge ($Z(500hPa) > 5700m$) by $$T = T - \frac{5}{\sigma_p} \cdot |T - \mu_p| \cdot \frac{5 * \sigma_Z}{|Z - \mu_Z|} \quad (5.3)$$
Cool inside ridge	Cooled areas of the stratosphere by selecting a polygon around the block, and when (x,y) is in the polygon, $$T = T - \frac{8\sigma_Z}{|Z - \mu_Z| \cdot \sigma_p} \cdot |T - \mu_p| \quad (5.4)$$
Cool all lower troposphere	Cooled entire lower troposphere by 10K.
Cool troposphere by height	Cooled areas of the lower troposphere by *eqn. 5.3*
Cool troposphere inside ridge	Cooled areas of the lower troposphere by *eqn 5.4*
Cool height change	Cooled 15°x 15°area of stratosphere above the fastest 12-hour 500 hPa height change by *eqn 3.1* with $n = -5$

This is supported by the time series of averaged integrated adiabatic and advective temperature change (*fig. 5.3 & 5.4*) where the vertical line represents the time of onset. In both graphs, the modification has reduced in magnitude the height change as a result of thermal processes, but most notably, the adiabatic term outweighs the advective term for both modified and unmodified. The total height change seen in *figure 5.2* is reduced at nearly all times.

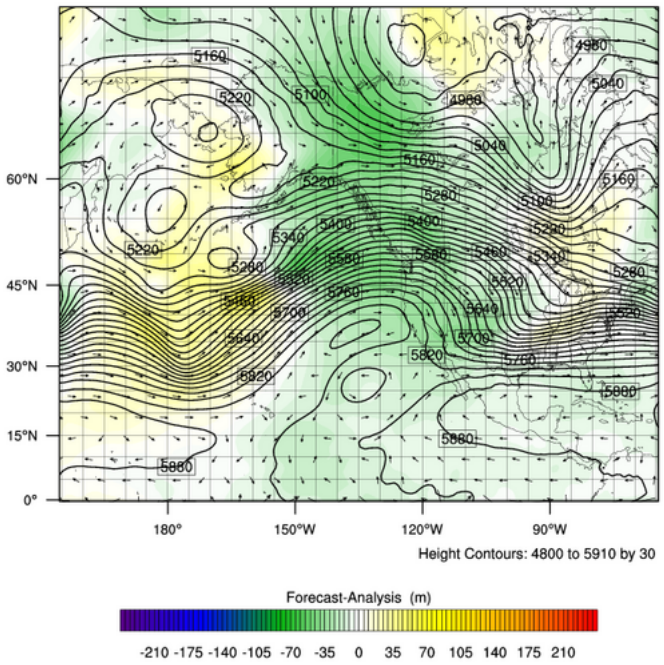

Figure 5.1: 1200Z 10 Jan 2009, 500 hPa modified heights (m) contoured, Modified Height-Analysis Height shaded (m)

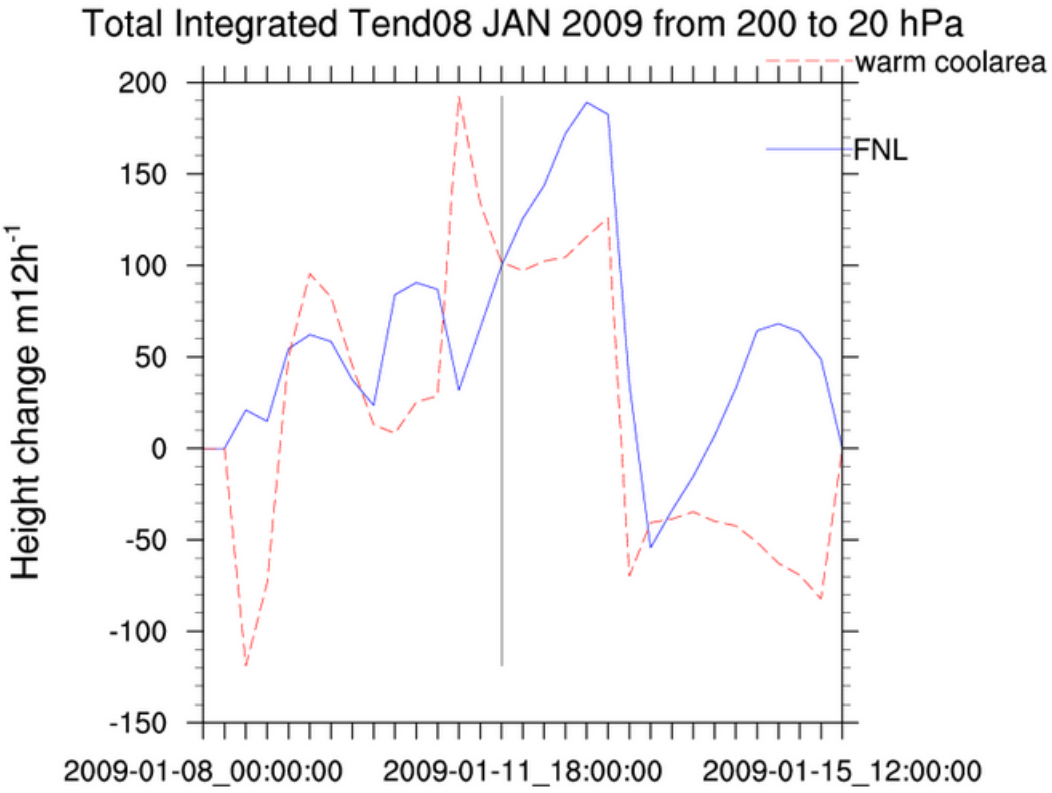

Figure 5.2: Integrated total temperature change for warming the cool area at onset. Vertical line indicates onset.

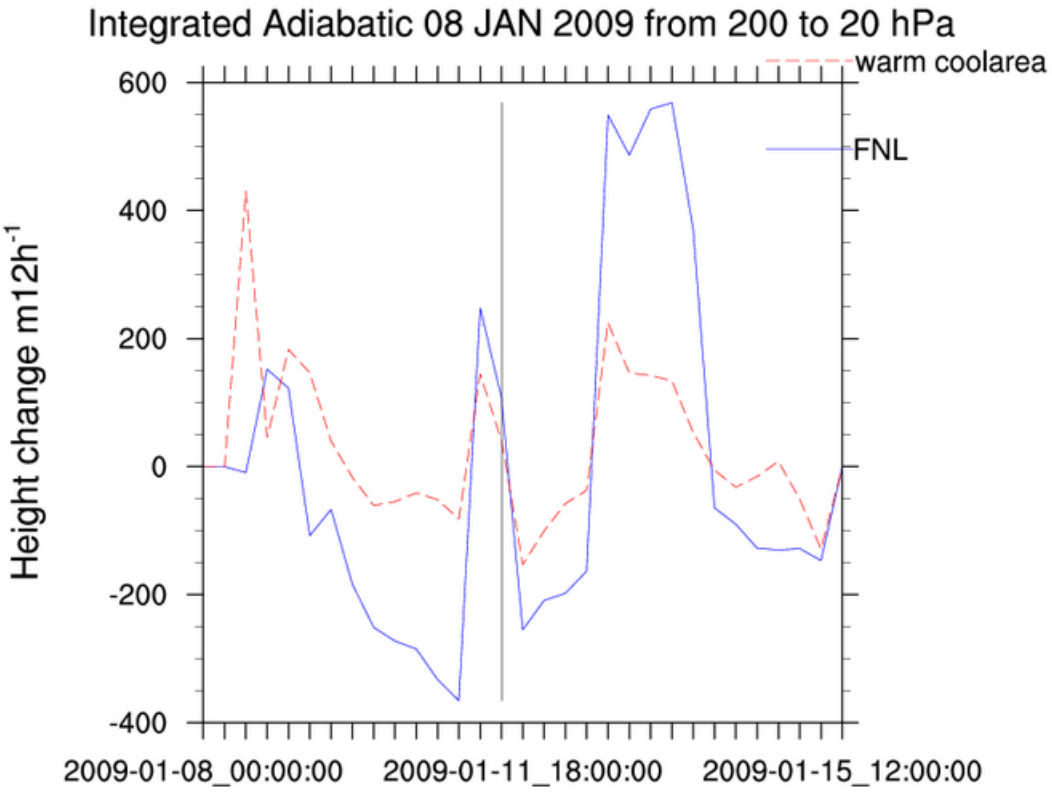

Figure 5.3: Integrated adiabatic temperature change for warming the cool area at onset. Vertical line indicates onset.

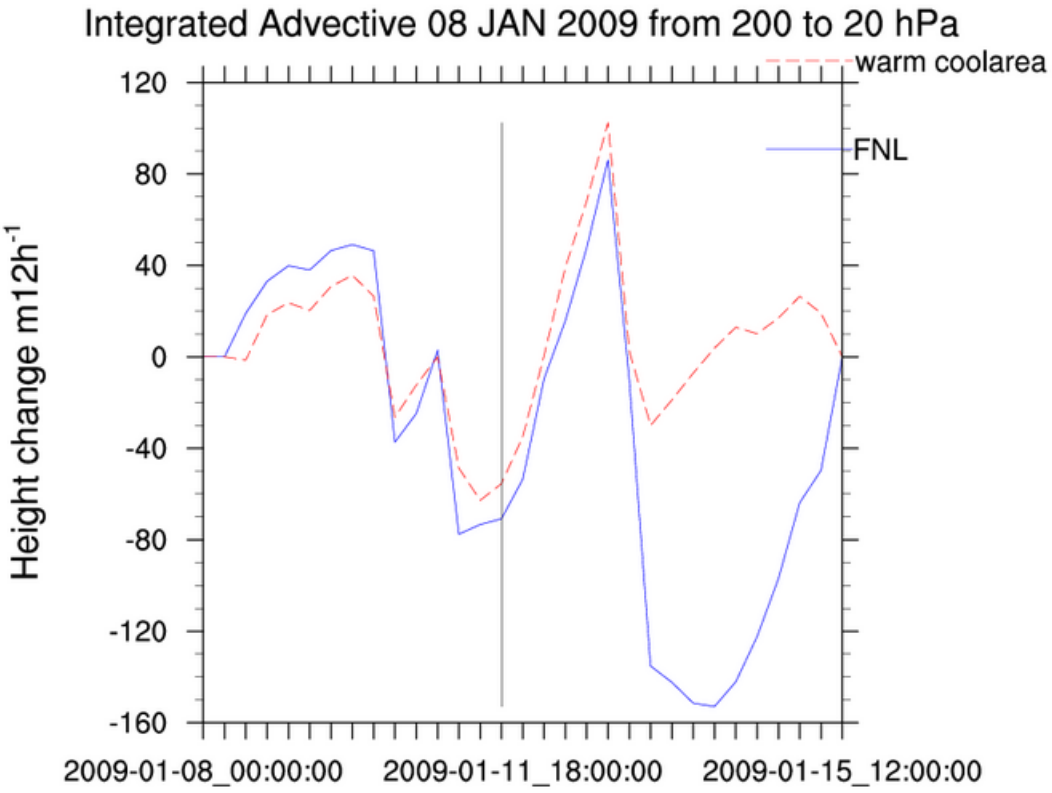

Figure 5.4: Integrated advective temperature change for warming the cool area at onset. Vertical line indicates onset.

5.1.2 Warming inside ridge

The in-ridge warming took place in a polygon that surrounded the mature blocking ridge, seen in *figure C.2*. Counter-intuitively, this had little effect on the formation of the block. The block onset was weakened, but not as much as it was during the warming of the cool area (compare *fig. 5.1 and 5.5*). As illustrated before *figures 5.7& 5.8* show the integrated adiabatic and advective height changes. With only a few exceptions, the advective graph is as expected, less than the final analysis. In the adiabatic term, the height change is first increased, then during the final two days of the block, decreased significantly, also seen in the total height change in *figure 5.6*. This is also where the biggest impact on the total height change is seen, exhibited in *figure 5.9*.

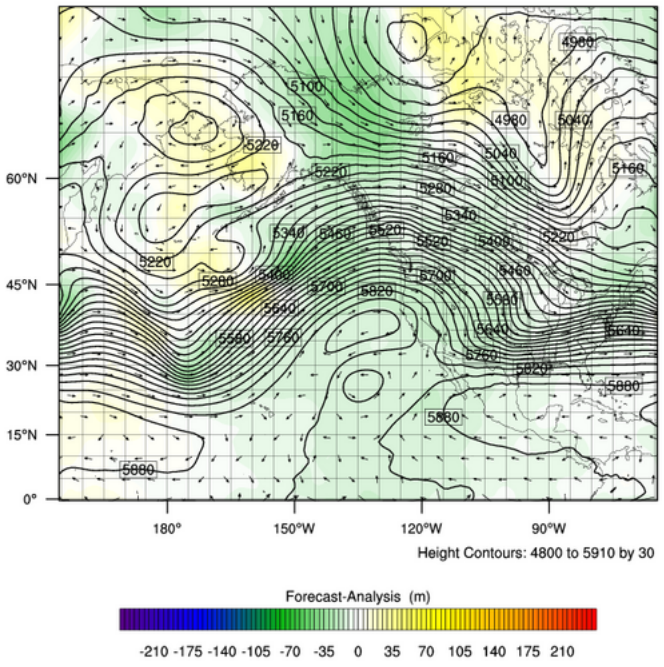

Figure 5.5: 1200Z 10 Jan 2009, 500 hPa modified heights (m) contoured, Modified Height-Analysis Height (m) shaded

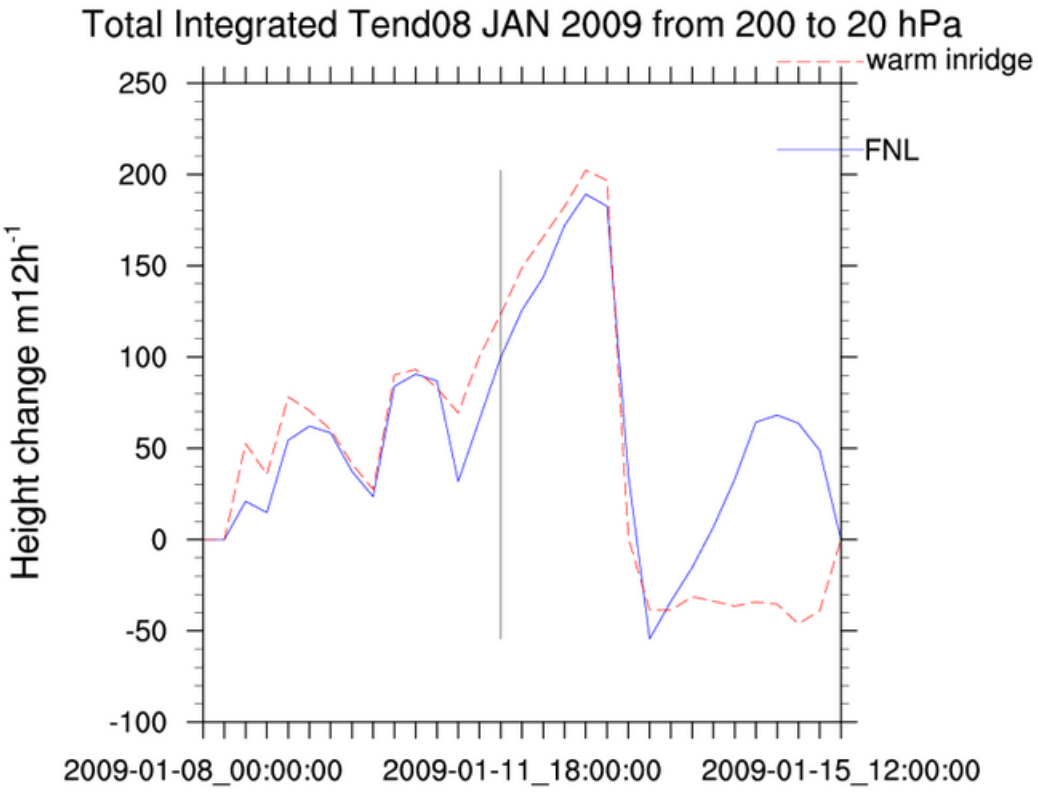

Figure 5.6: Integrated total temperature change for Warming inside the ridge at onset. Vertical line indicates onset.

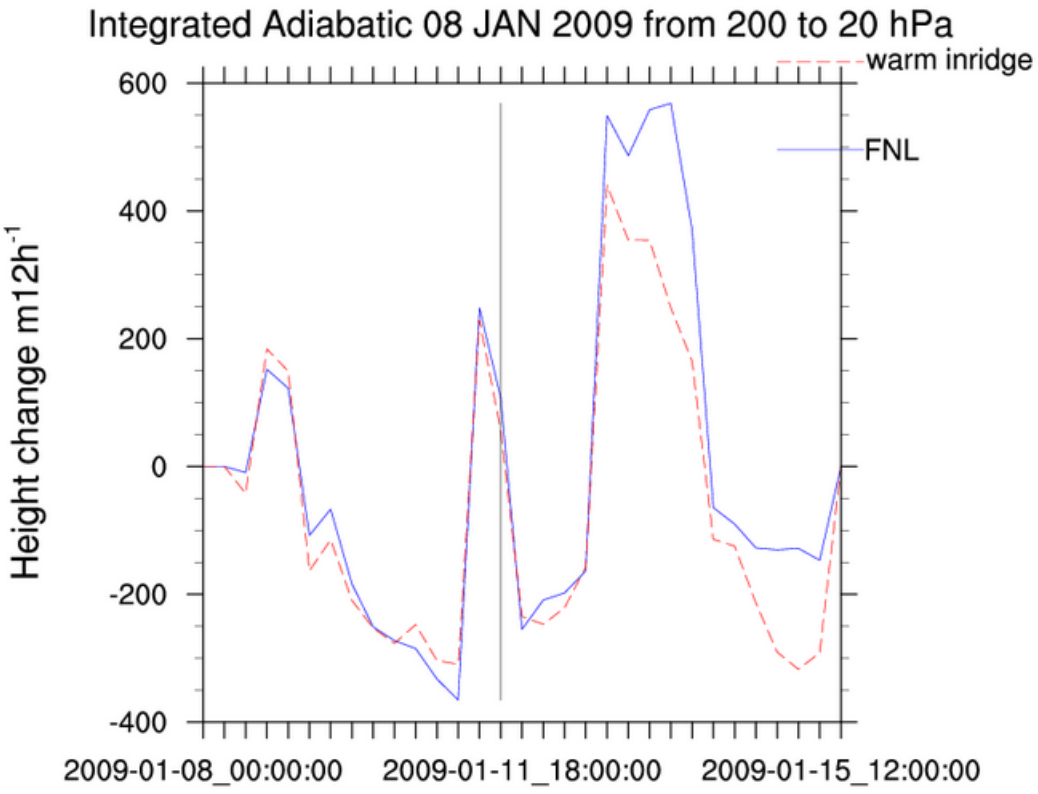

Figure 5.7: Integrated adiabatic temperature change for Warming inside the ridge at onset. Vertical line indicates onset.

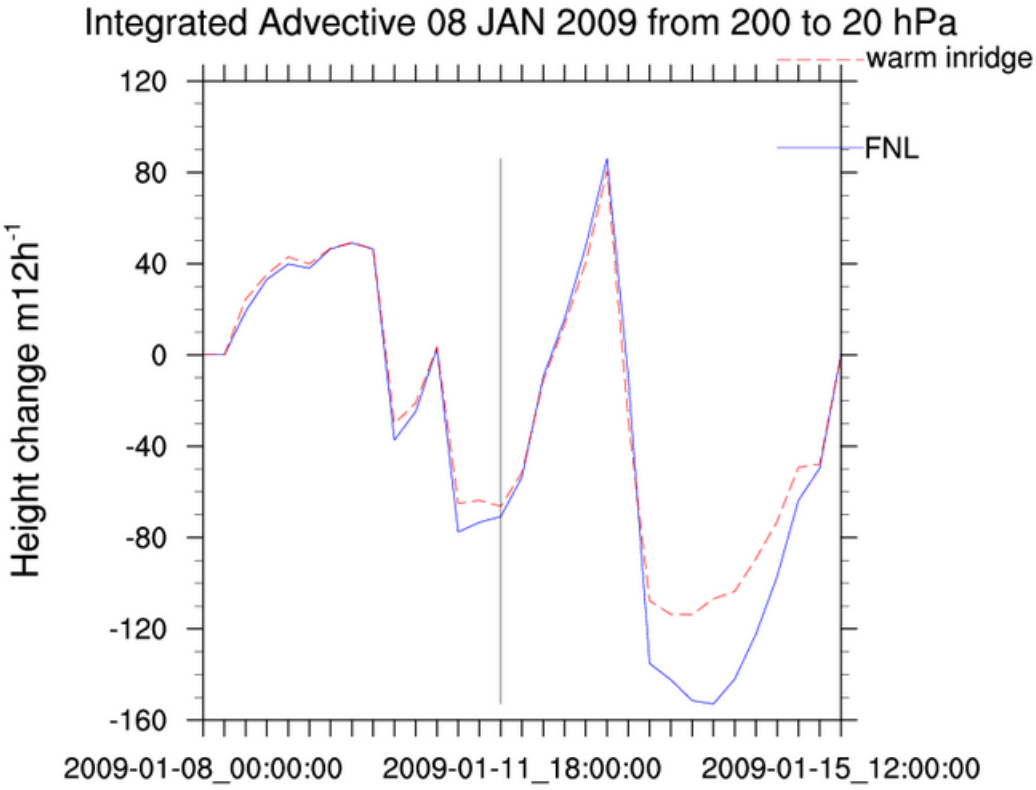

Figure 5.8: Integrated advective temperature change for Warming inside the ridge at onset. Vertical line indicates onset.

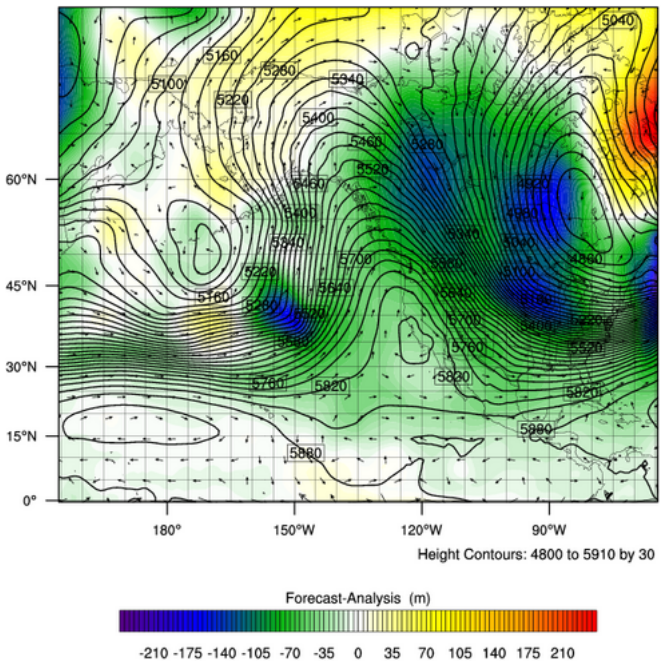

Figure 5.9: 1800Z 14 Jan 2009, 500 hPa modified heights (m) contoured, Modified Height-Analysis Height (m) shaded

5.1.3 Warming the troposphere by height

In this modification, undertaken for comparison to stratospheric modification, the model produced a different response in the 500 hPa height field. During the two stratospheric modifications mentioned, the sign of the height change (negative in the warming cases) was constant within the ridge. In the tropospheric warming case, the heights of the modified run increased on the east side of the ridge, and decreased on the west as seen in *figure 5.10*. This modification also reduced, at almost all times, the total thermally forced height change over the fastest height change, seen in *figure 5.11*. This is the opposite of the expected result, warming in the lower tropsphere should cause an increase in heights. However, at the fastest height change point, the height rises were reduced.

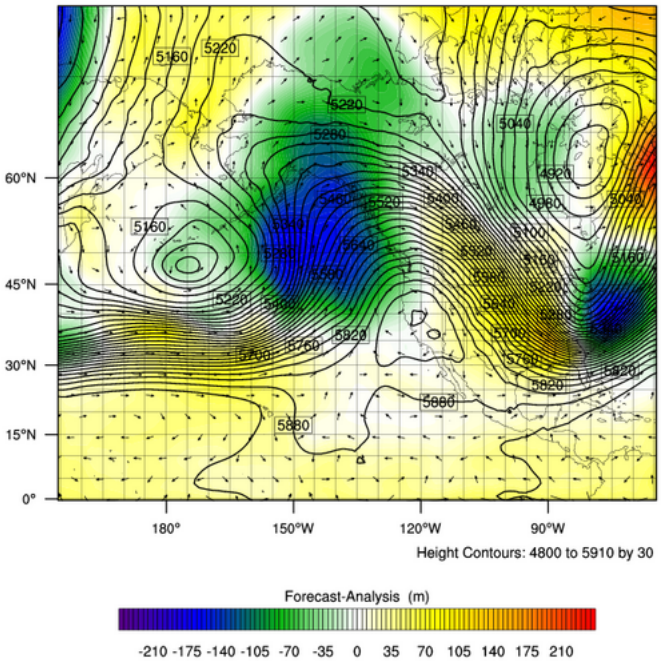

Figure 5.10: 0000Z 14 Jan 2009, 500 hPa modified heights (m) contoured, Modified Height-Analysis Height (m) shaded

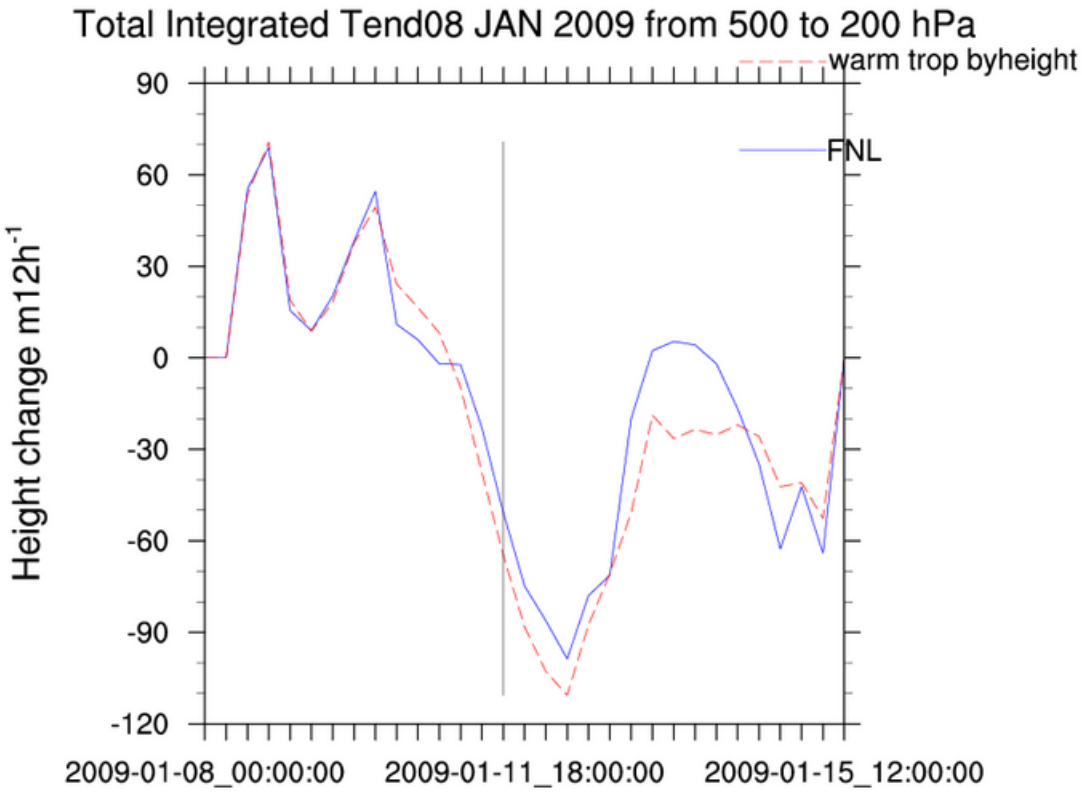

Figure 5.11: Integrated total temperature change for Warming troposphere by height at onset. Vertical line indicates onset.

5.1.4 Warming height change

To produce a change in the averaged integrated adiabatic and advective height change terms, the temperature in the stratosphere was warmed over a 15°x 15°area centered on the fastest 12 hour height rises. The 15°x 15°area was used because modifying the 10°x 10°area had no discernible effect. This warming should, in theory, decrease the height rises, specifically over the 10°x 10°area over which the averages were calculated. As seen in *figures 5.15 & 5.16*, this was

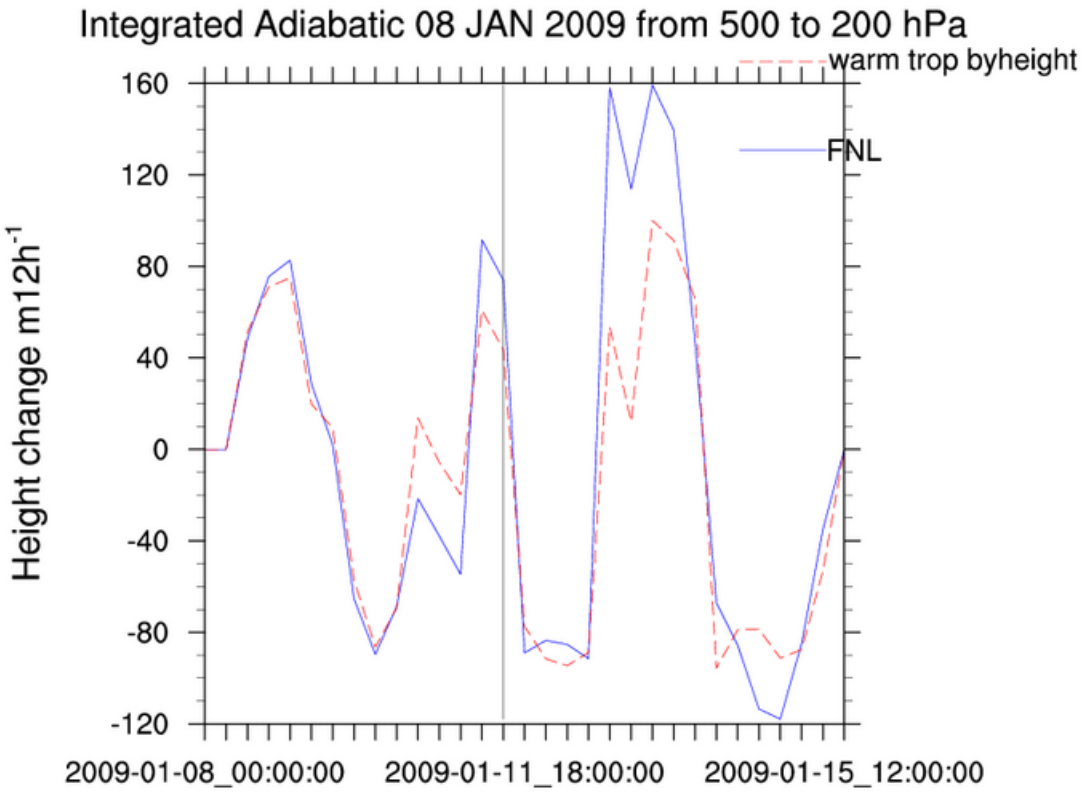

Figure 5.12: Integrated adiabatic temperature change for Warming troposphere by height at onset. Vertical line indicates onset.

not strictly the case. In the adiabatic term, the change is in the positive direction, but eventually recovers to be below or near the final analysis curve. In the advective term, however, the change is as expected, a strongly negative reaction within the first few time frames, and remaining mostly below the final analysis for the rest of the run. This is evident in the difference between the modified forecast and analysis seen in *figure 5.17*, where the onset of the block is weaker, as expected. In the total height change, *figure 5.14*, the inital difference in height rises is quite large, possibly due to model spin up, then recovers and matches

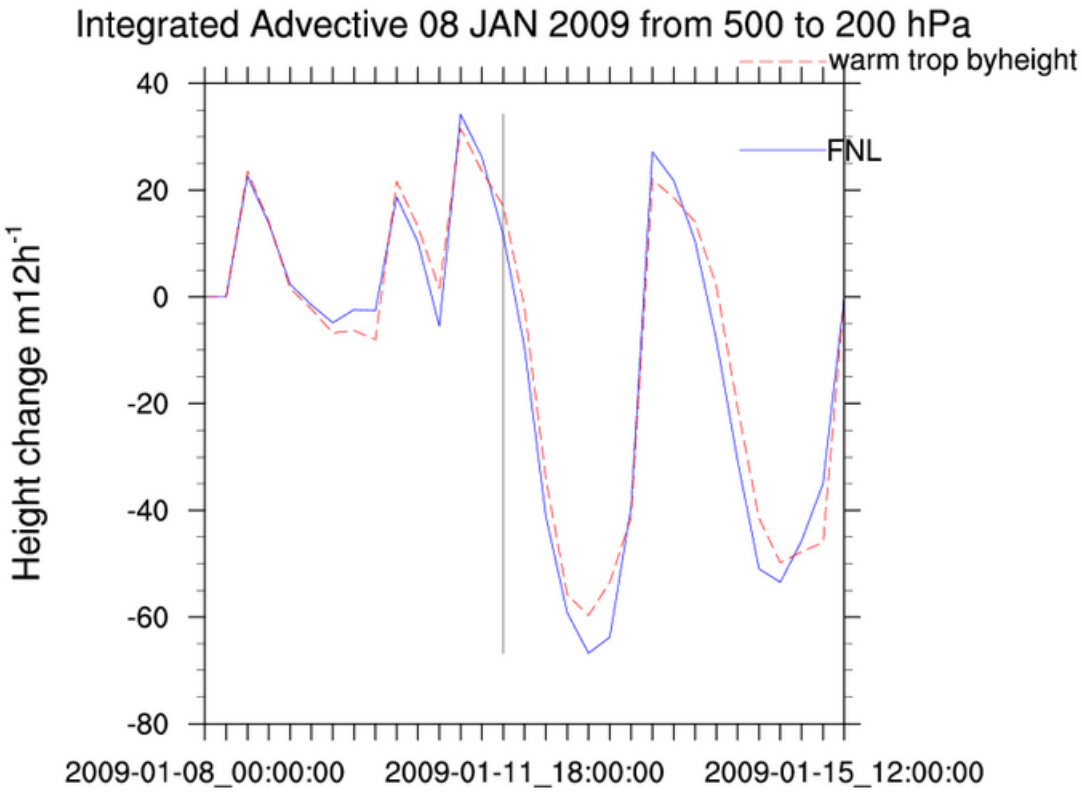

Figure 5.13: Integrated advective temperature change for Warming troposphere by height at onset. Vertical line indicates onset.

well with the component terms.

5.1.5 Cooling height change

This modification was used to compare against the warming runs, and in theory should produce increased height rises and strengthen the block at onset. The adiabatic height change (*fig. 5.19*) only increased in the day surrounding

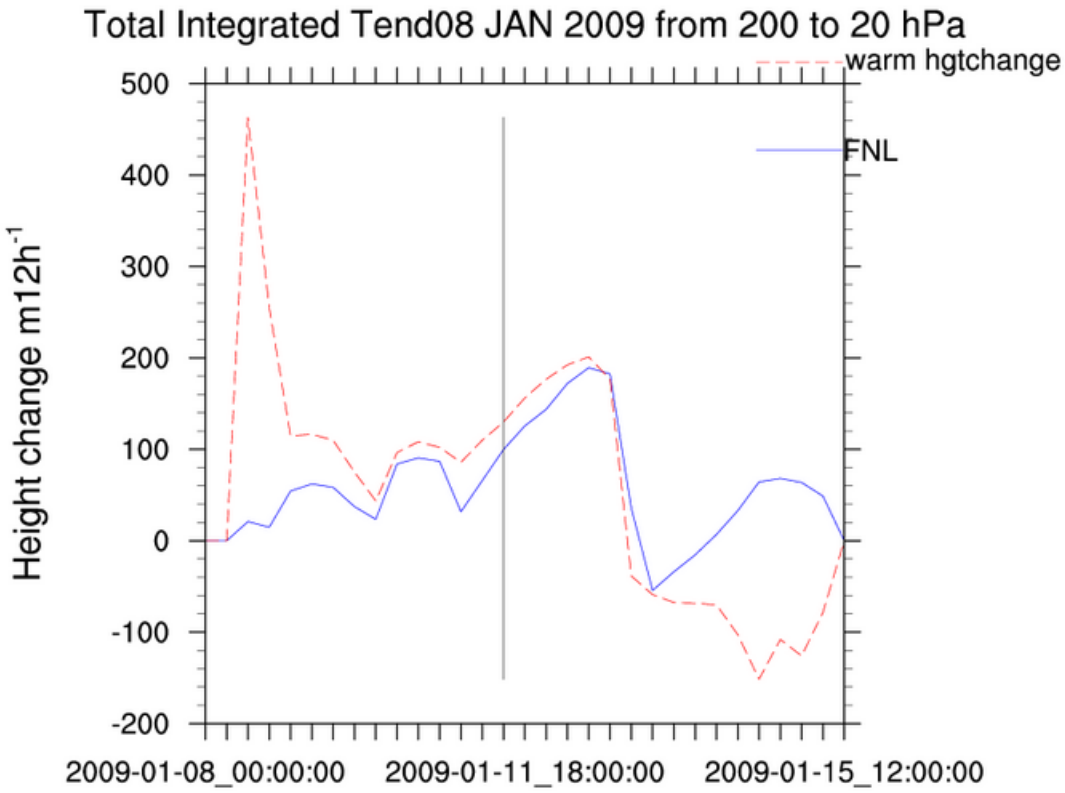

Figure 5.14: Integrated total temperature change for warming fastest height change at onset. Vertical line indicates onset.

the onset time, but was reduced almost everywhere else . The advective term (*fig. 5.20*), however, marginally increased at nearly every time. This did not, however, translate into a stronger block (*fig 5.21*); there were areas of strengthened heights, but not within the blocking high. Total height rises were increased post-breakdown seen in *figure 5.18*.

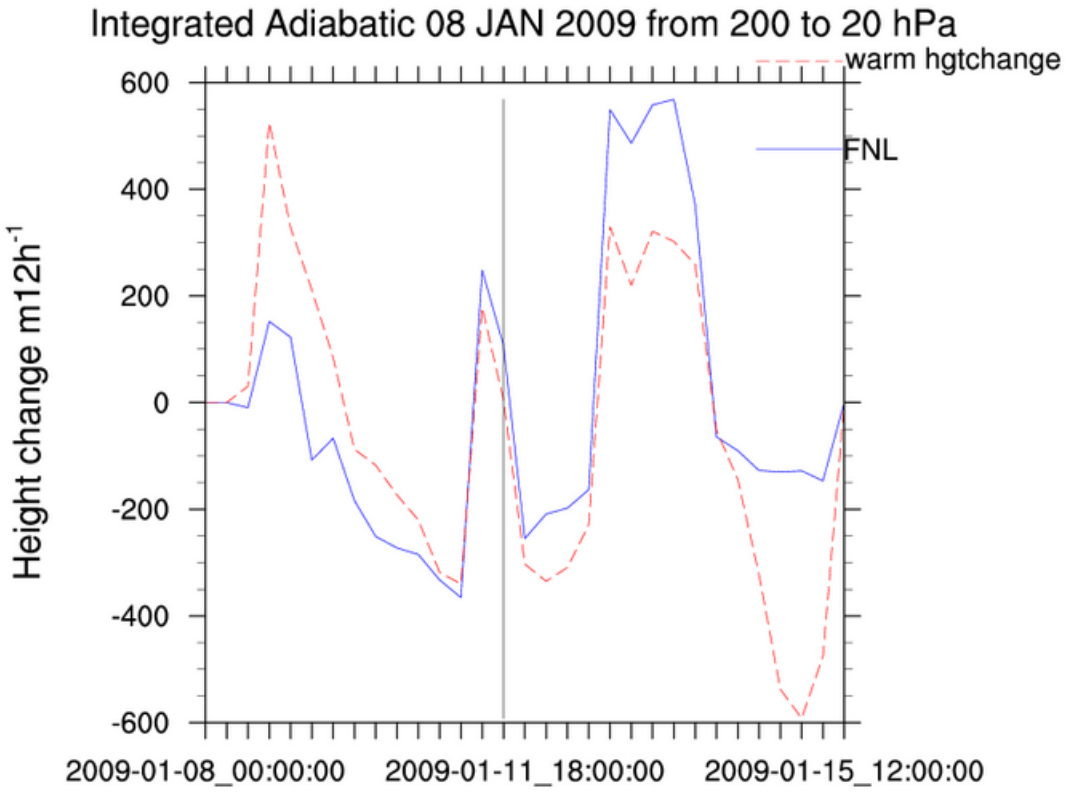

Figure 5.15: Integrated adiabatic temperature change for warming fastest height change at onset. Vertical line indicates onset.

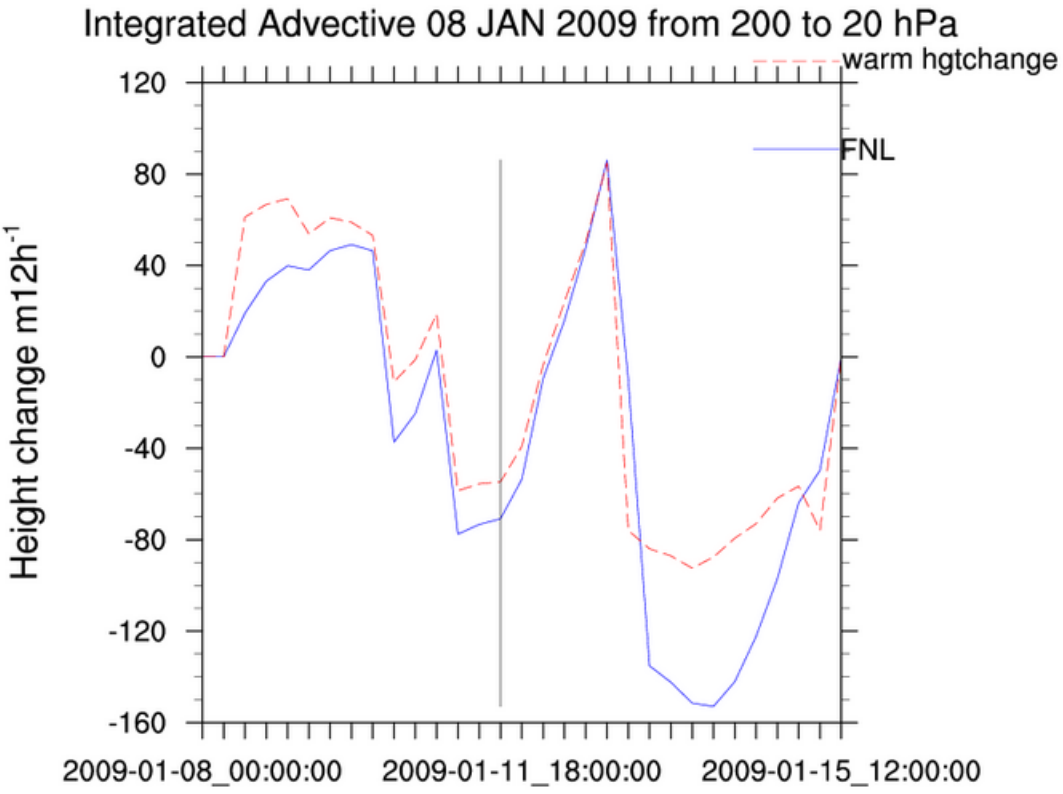

Figure 5.16: Integrated advective temperature change for warming fastest height change at onset. Vertical line indicates onset.

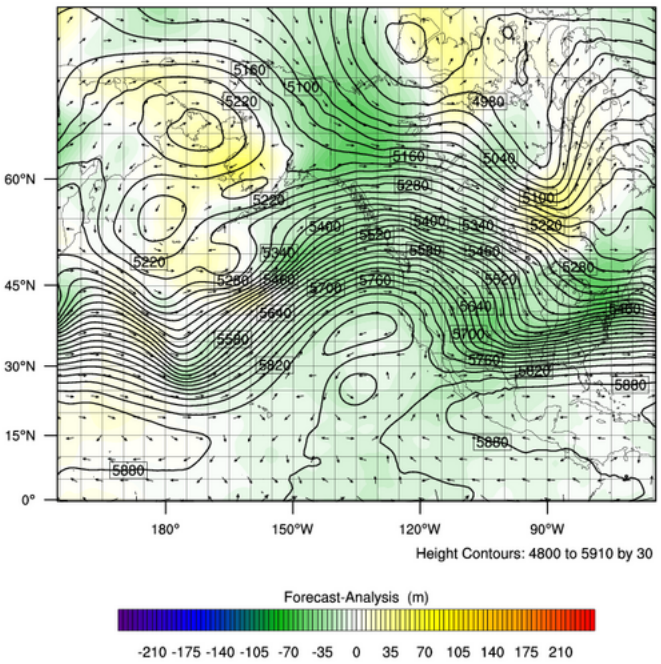

Figure 5.17: 1200Z 10 Jan 2009, 500 hPa modified heights (m) contoured, Modified Height-Analysis Height (m) shaded for warming height change at onset.

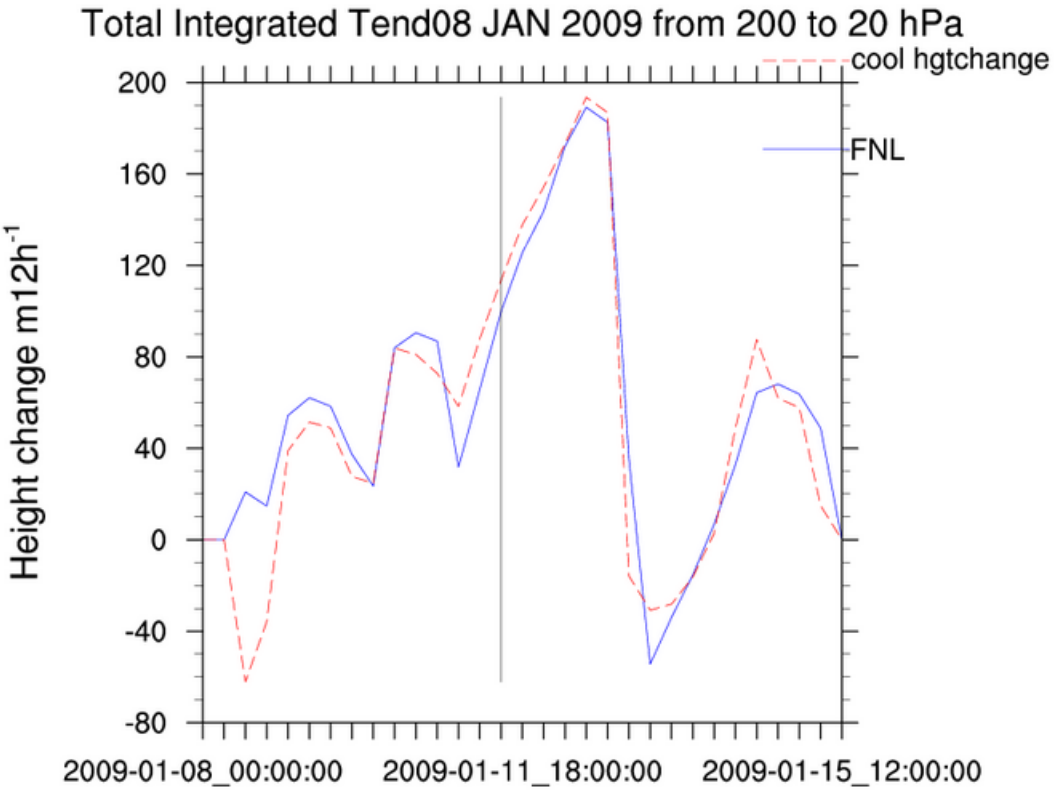

Figure 5.18: Integrated total temperature change for cooling fastest height change at onset. Vertical line indicates onset.

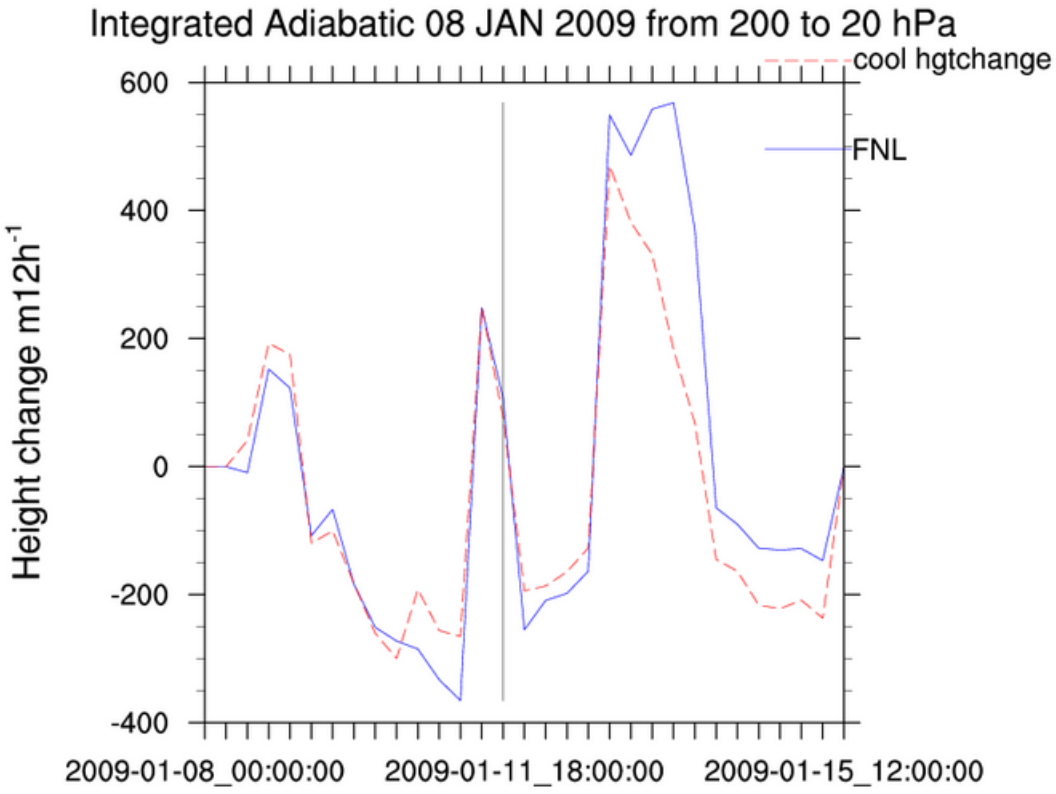

Figure 5.19: Integrated adiabatic temperature change for cooling fastest height change at onset. Vertical line indicates onset.

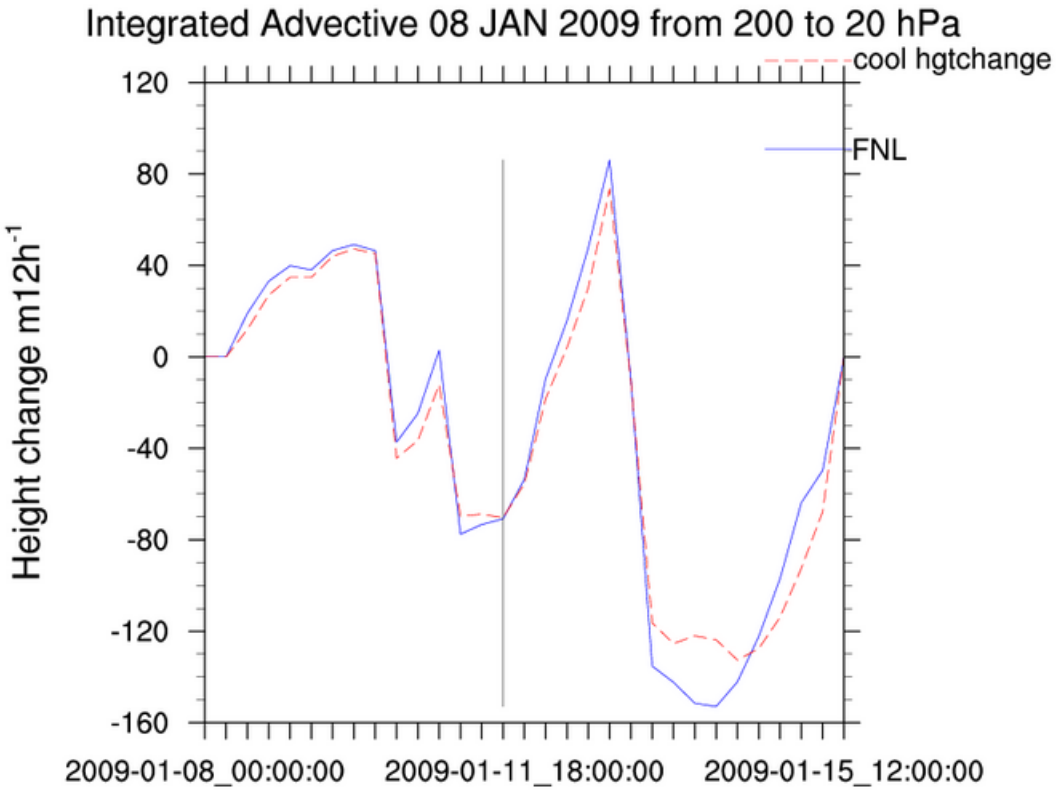

Figure 5.20: Integrated advective temperature change for cooling fastest height change at onset. Vertical line indicates onset.

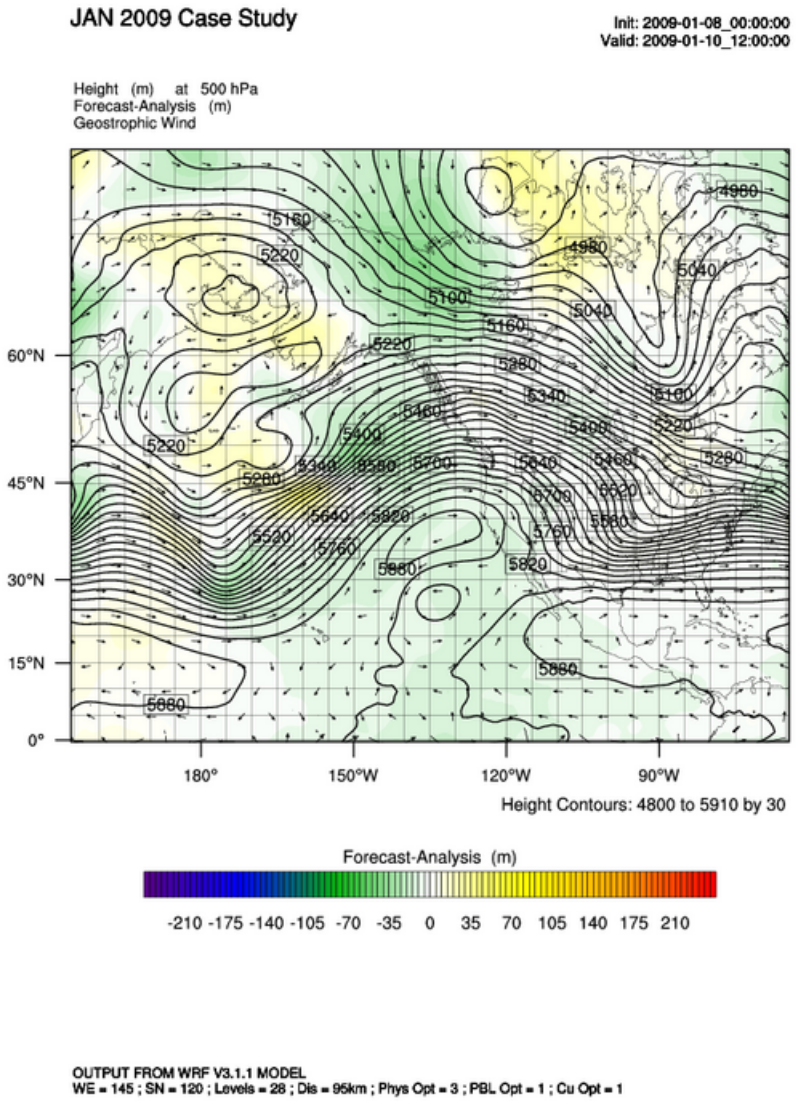

Figure 5.21: 1200Z 10 Jan 2009, 500 hPa modified heights (m) contoured, Modified Height-Analysis Height (m) shaded for cooling height change at onset.

5.2 Breakdown

5.2.1 Cooling warm area

The first breakdown run to be examined is the cooling of the warm area. The hypothesis is that this modification would produce a longer lasting block due to increased adiabatic and advective cooling. This was the case, because as seen in *figure 5.22*, the block lasted approximately 12 hours longer after modification than in the final analysis. In the integrated temperature graphs, however, this result is not evident. This is most noticeable in the adiabatic term (*fig. 5.24*); within the first 36 hours, the height rises are increased, however, after block onset the height rises are reduced, or height falls are increased. It can also be seen in the total height change *figure 5.23* that height falls are increased by the modification. This effect is observed over the fastest height change, not necessarily a location whose temperature was directly modified. In this case, there may have been a counter-modification made during the WRF model run that attempted to correct for the modification made.

5.2.2 Cooling inside ridge

This modification took place inside the ridge in the same way that the block was warmed during onset. This should produce a greater effect than that of the warming of the cool area, as it specifically targets the blocking ridge. This was not the case; the block lasted approximately 12 hours longer than in the final analysis, which is the same as it did for the cooling of the warm area. The integrated adiabatic height change graph shows that while there was an increase

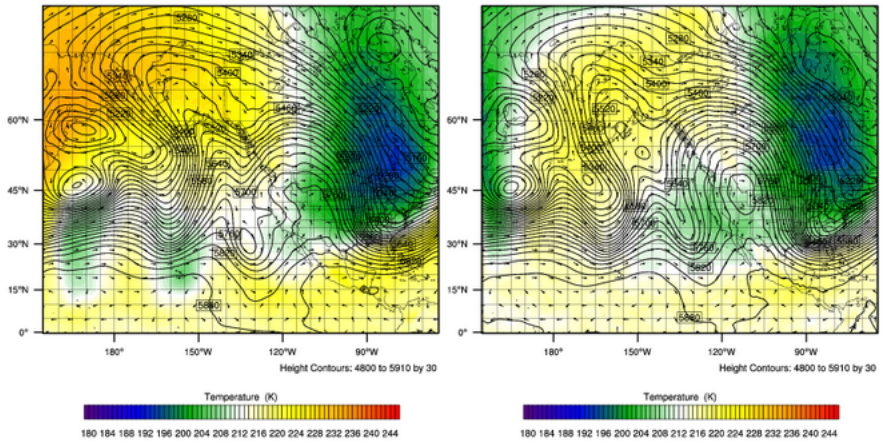

Figure 5.22: 1800Z 20 Jan 2009, 500 hPa modified heights (m) contoured, 20 hPa temperature (K) shaded. FNL on left, Cooled warm area on right.

in height rises at the breakdown time, after breakdown the height rises sharply drop into height falls (*fig. 5.27*), whereas in the total height change, the cooling modification has forced height falls to increase (*fig. 5.26*).

5.2.3 Cooling the troposphere by height

This modification was used to compare tropospheric effects to stratospheric effects at breakdown. The lower troposphere was cooled where the 500 hPa heights were greater than 5700m. The expectation is for height falls to be increased due to cooling in the lower troposphere. This effect did not take place as predicted, but changes can be seen in the integrated terms; for some time periods the change is towards height rises, but most times it is towards height falls (*fig. 5.29, fig. 5.30 and fig. 5.31*). Despite this, the block was forecasted to last for an additional 12 hours after breakdown. As seen in *figure 5.32* the area of the troposphere underneath the continued block is warmer than in the final

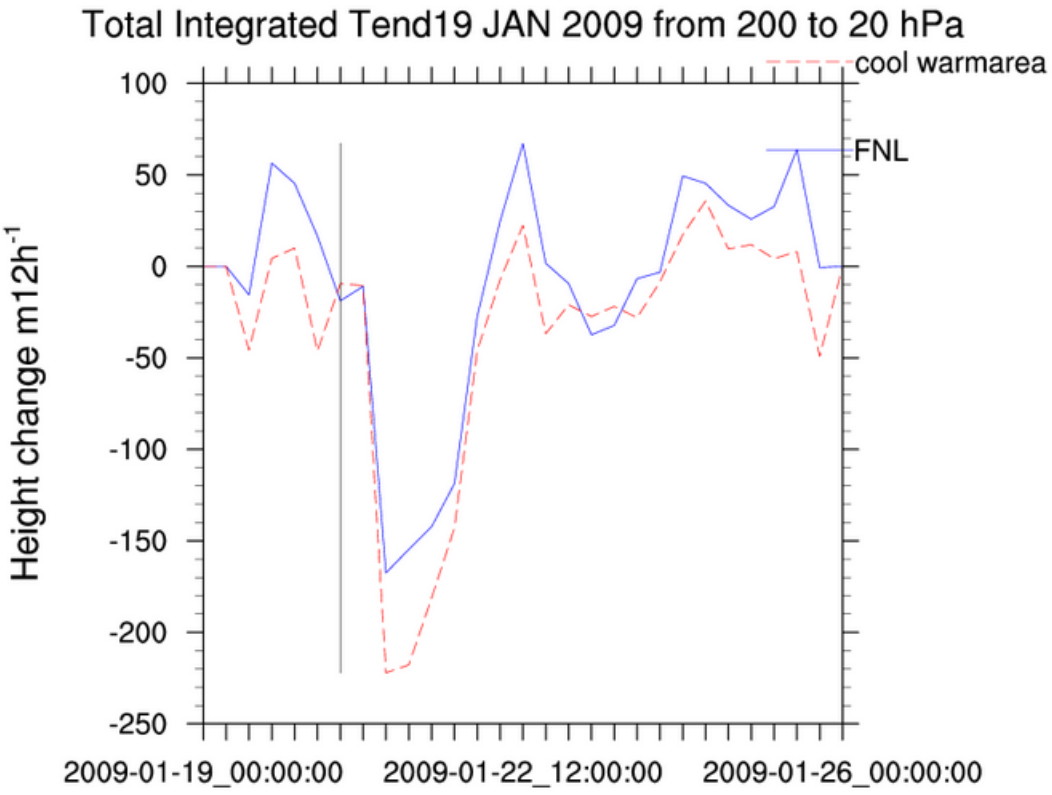

Figure 5.23: Integrated total temperature change for cooling the warm area at breakdown. Vertical line indicates breakdown.

analysis. Thus again there is a balancing effect taking place within the model.

5.2.4 Cooling height change

Cooling over the fastest 12 hour height change was done in the same manner for breakdown as it was at onset. It did not, however, produce similar results. Block decay was delayed by 12 hours, but the change in both adiabatic and ad-

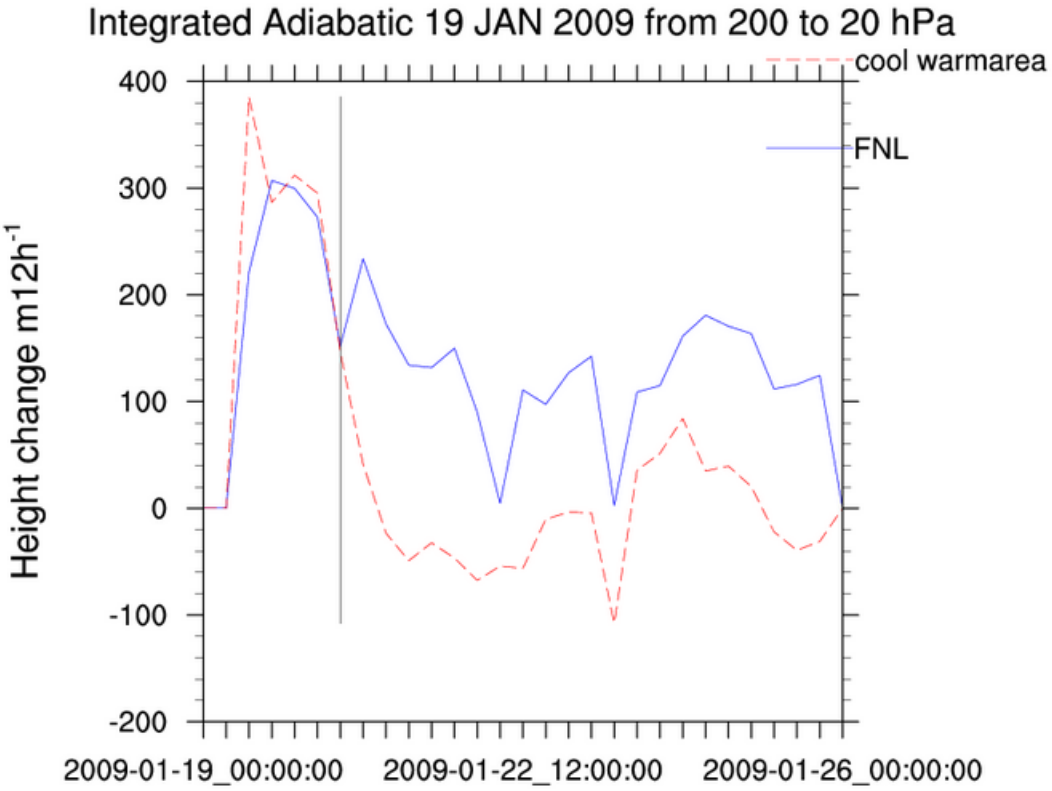

Figure 5.24: Integrated adiabatic temperature change for cooling the warm area at breakdown. Vertical line indicates breakdown.

vective terms was not unimodal. As seen in *figure 5.34 and 5.35*, both terms near breakdown were greater than in the final analysis, thus contributing to a longer lasting block, but did not remain that way as expected. This is again, potentially due to corrective behavior within the model, offsetting the modification, seen in the total height change term (*fig. 5.33*).

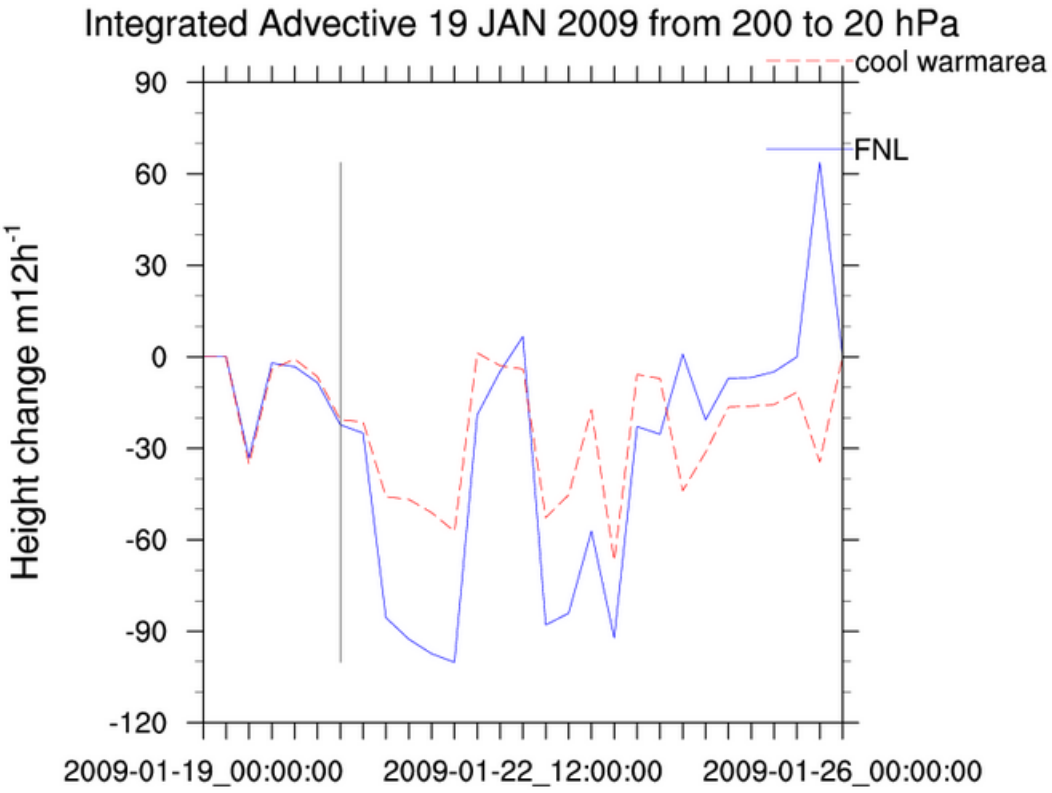

Figure 5.25: Integrated advective temperature change for cooling the warm area at breakdown. Vertical line indicates breakdown.

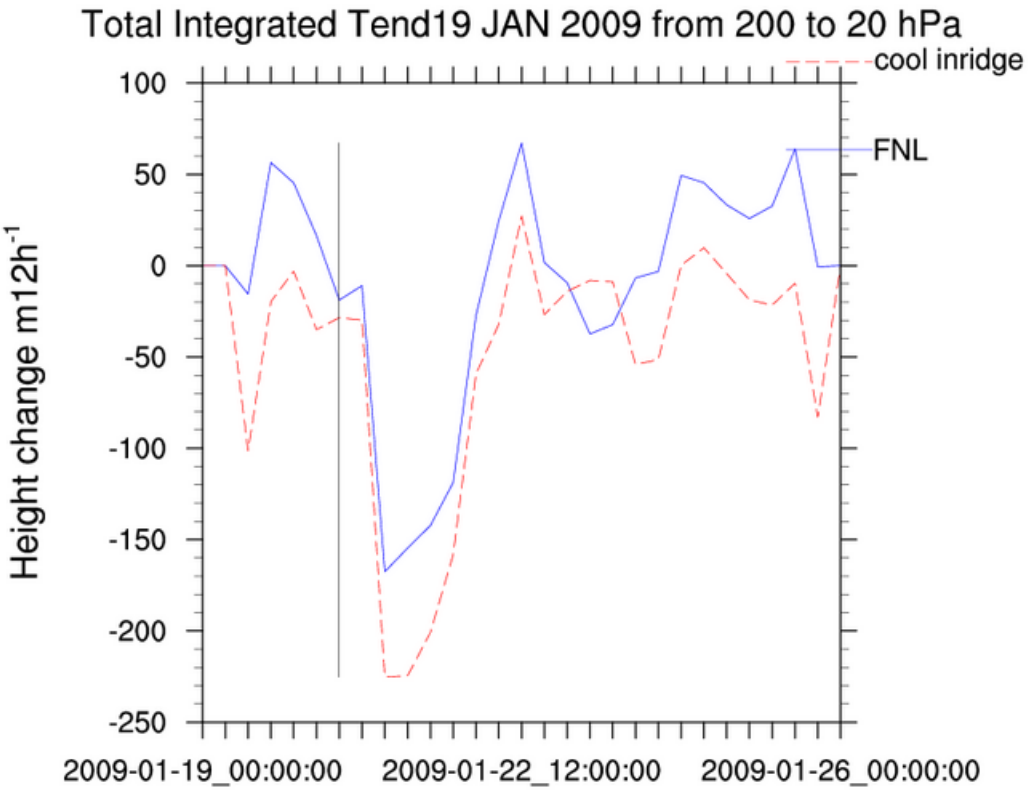

Figure 5.26: Integrated total temperature change for cooling inside the ridge at breakdown. Vertical line indicates breakdown.

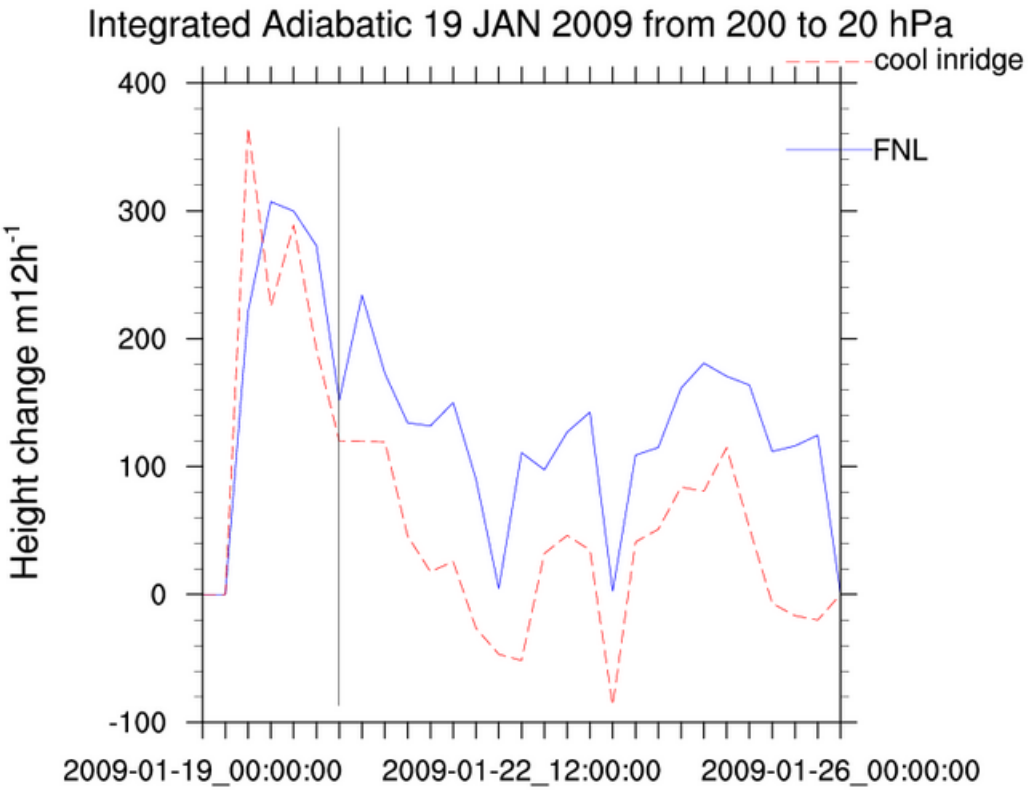

Figure 5.27: Integrated adiabatic temperature change for cooling inside the ridge at breakdown. Vertical line indicates breakdown.

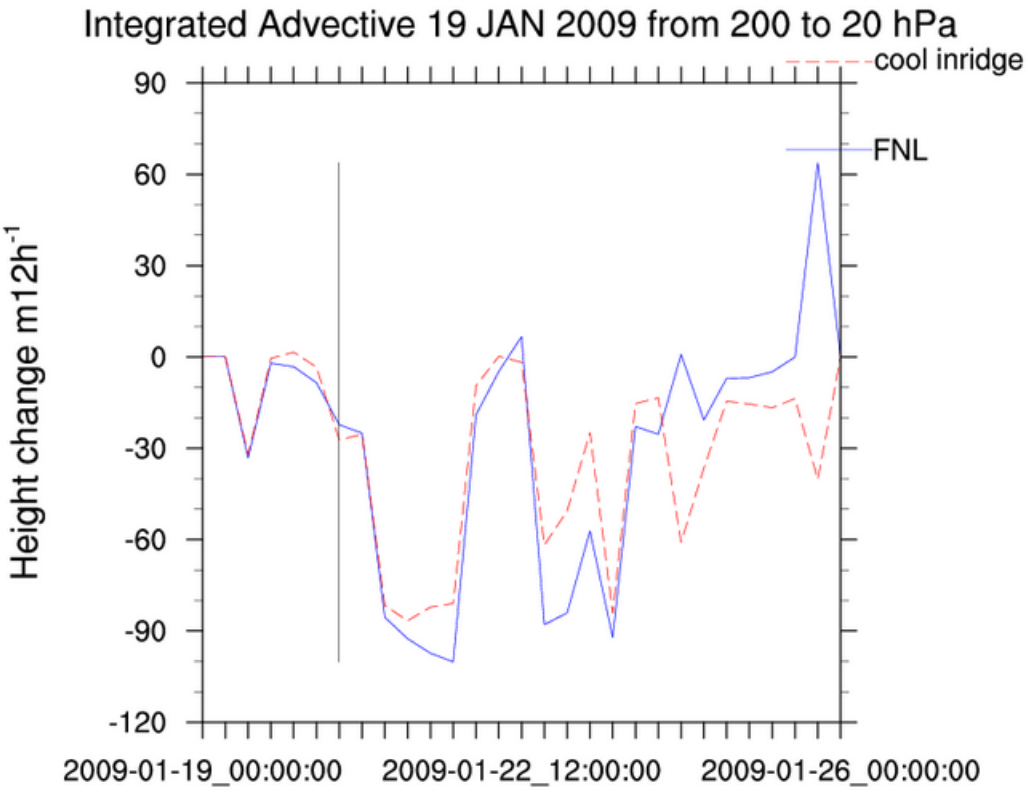

Figure 5.28: Integrated advective temperature change for cooling inside the ridge at breakdown. Vertical line indicates breakdown.

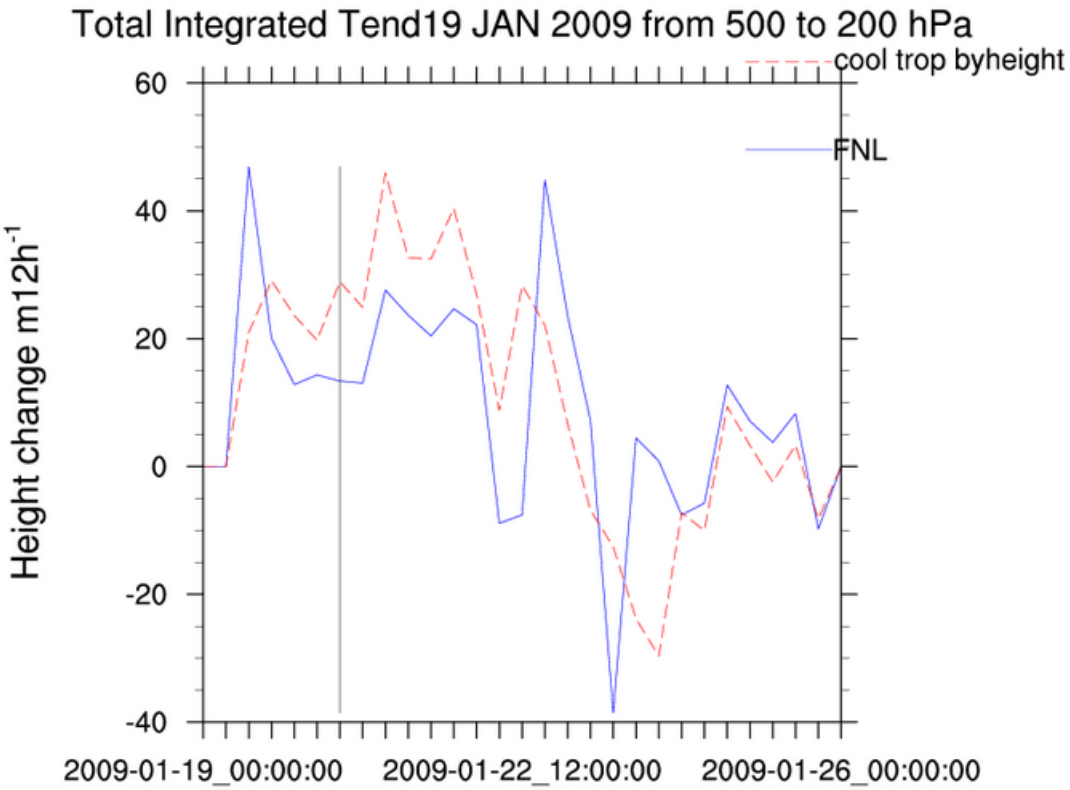

Figure 5.29: Integrated total temperature change for cooling the troposphere by height at breakdown. Vertical line indicates breakdown.

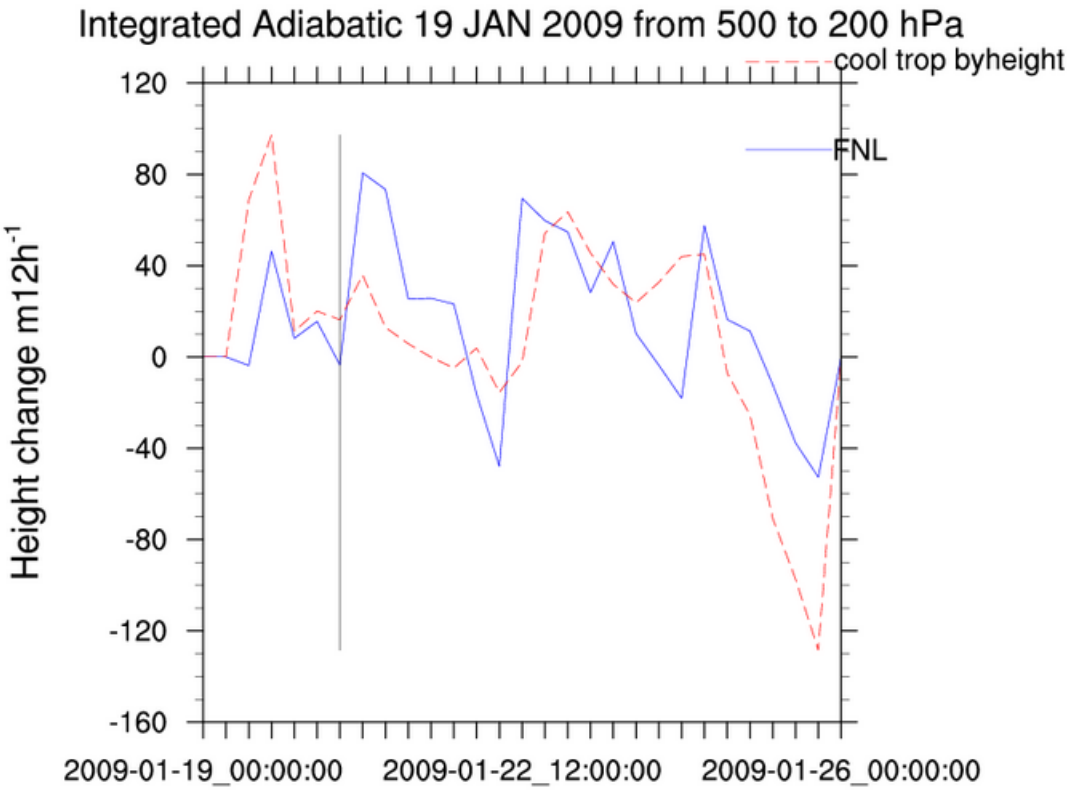

Figure 5.30: Integrated adiabatic temperature change for cooling the troposphere by height at breakdown. Vertical line indicates breakdown.

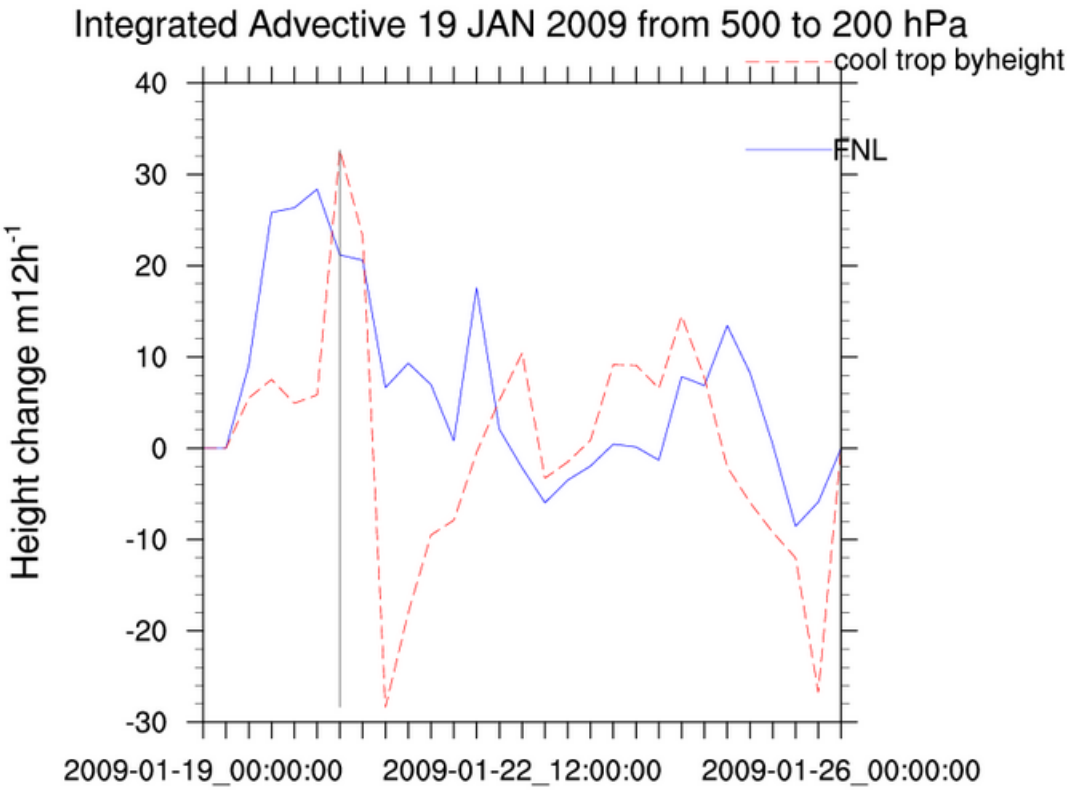

Figure 5.31: Integrated advective temperature change for cooling the troposphere by height at breakdown. Vertical line indicates breakdown.

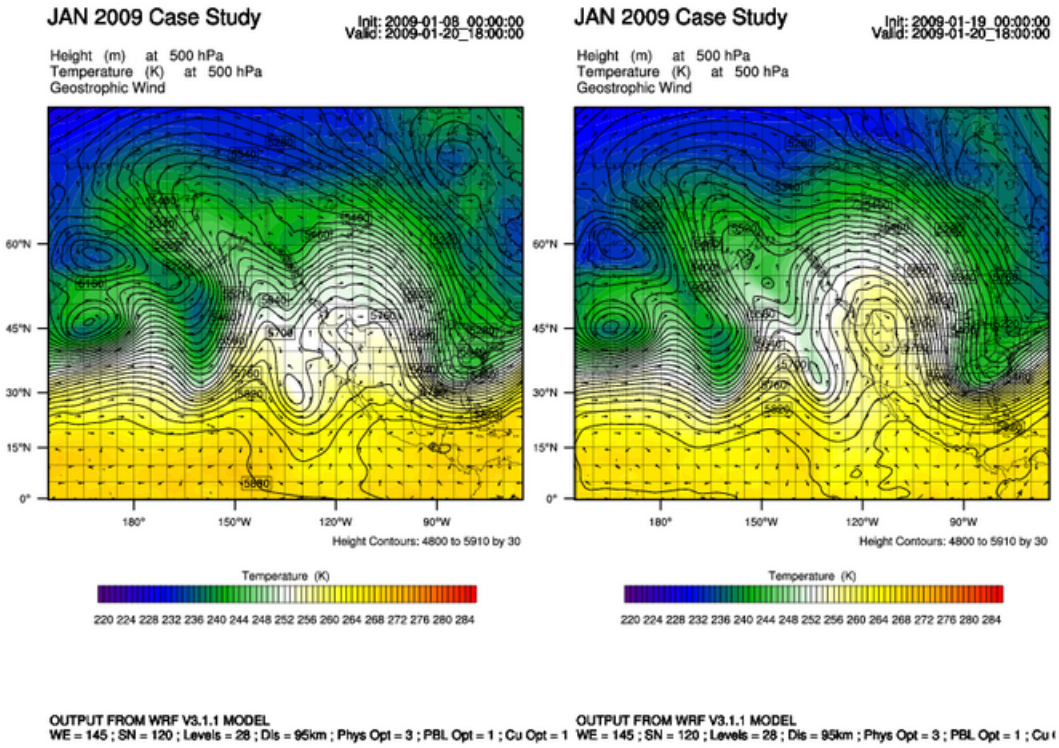

Figure 5.32: 1800Z 20 Jan 2009, 500 hPa modified heights (m) contoured, 500 hPa temperature (K) shaded. FNL on left, Cooled troposphere by height on right.

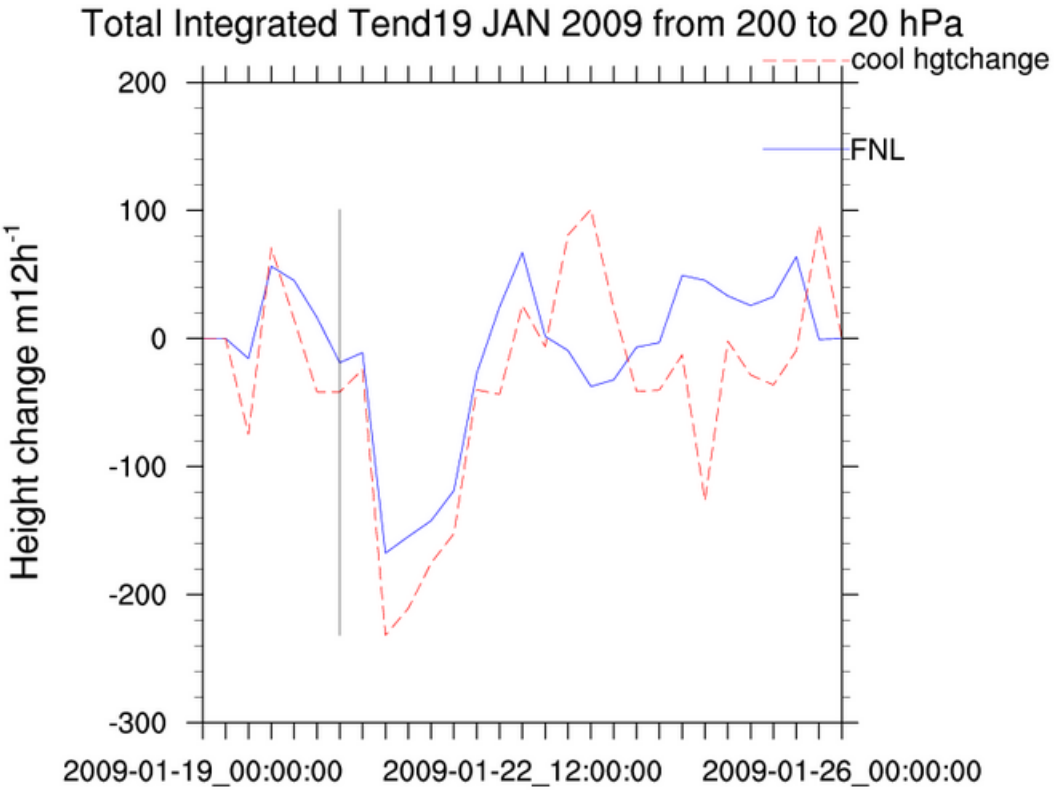

Figure 5.33: Integrated total temperature change for cooling the fastest height change at breakdown. Vertical line indicates breakdown.

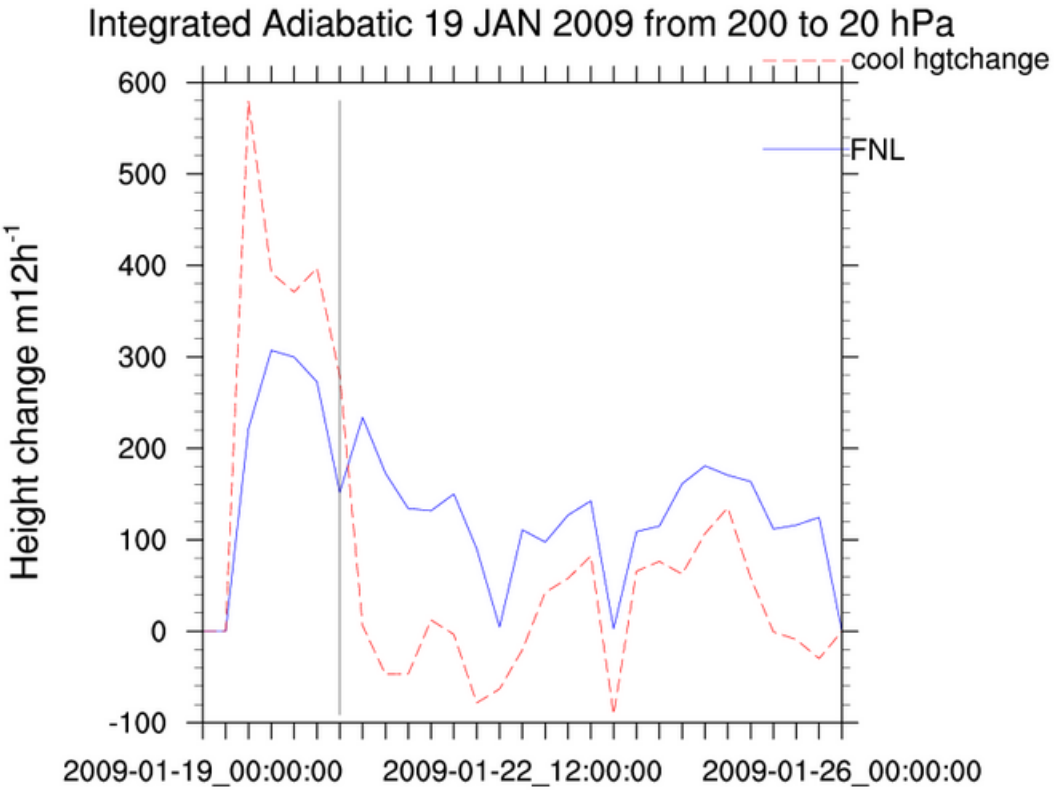

Figure 5.34: Integrated adiabatic temperature change for cooling the fastest height change at breakdown. Vertical line indicates breakdown.

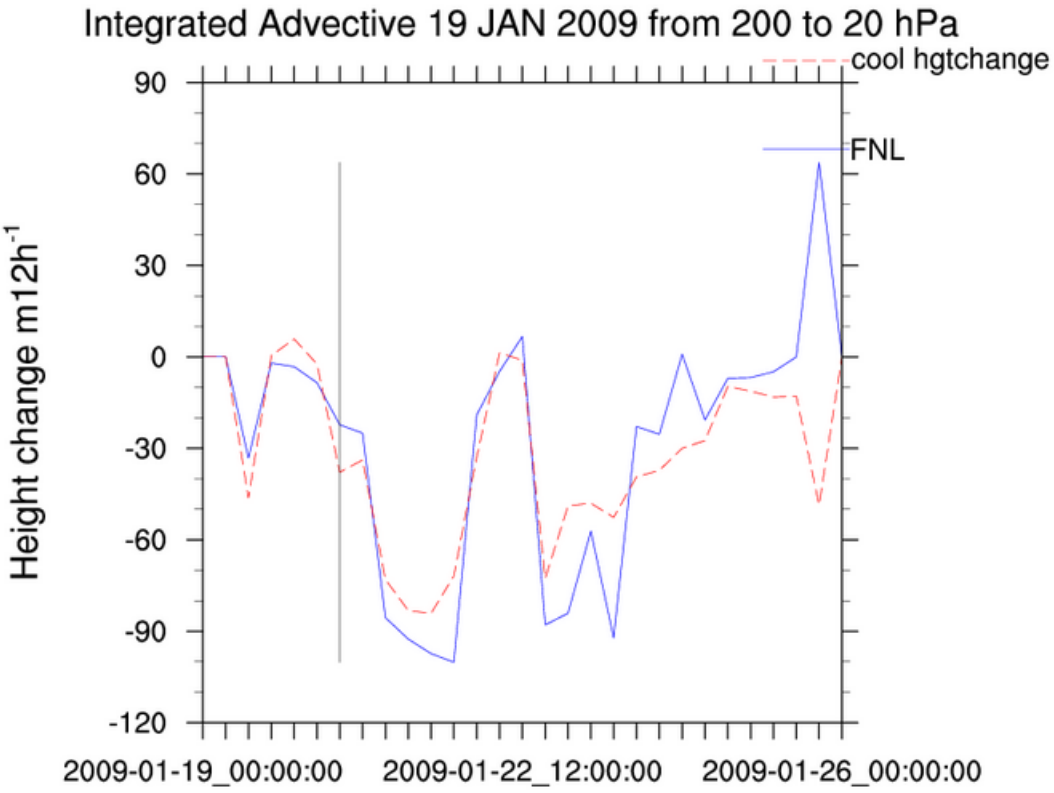

Figure 5.35: Integrated advective temperature change for cooling the fastest height change at breakdown. Vertical line indicates breakdown.

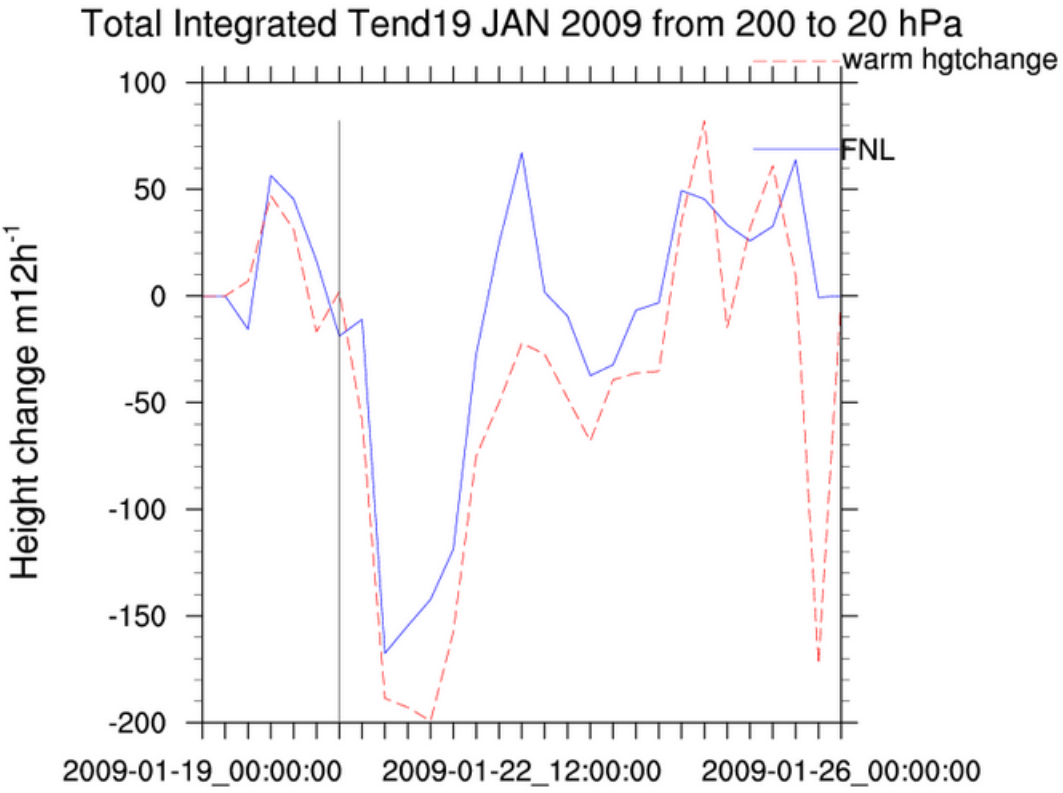

Figure 5.36: Integrated total temperature change for warming the fastest height change at breakdown. Vertical line indicates breakdown.

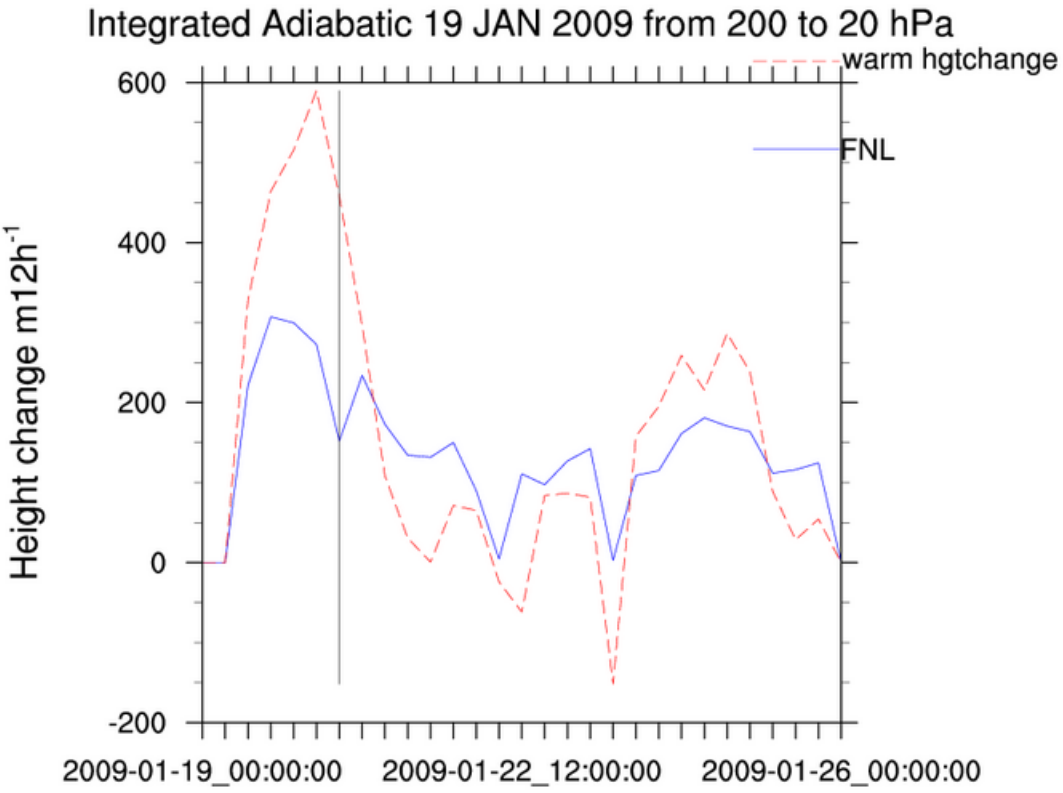

Figure 5.37: Integrated adiabatic temperature change for warming the fastest height change at breakdown. Vertical line indicates breakdown.

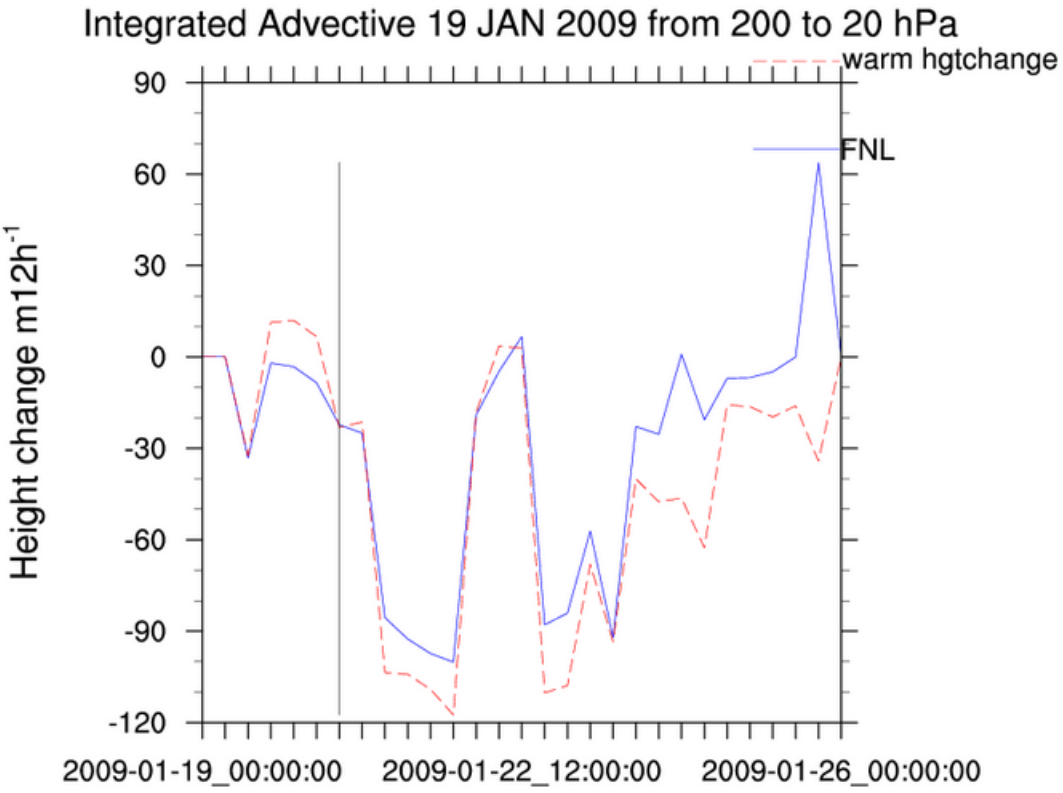

Figure 5.38: Integrated advective temperature change for warming the fastest height change at breakdown. Vertical line indicates breakdown.

5.2.5 Warming height change

Warming over the fastest 12 hour height change was also done in the same manner for breakdown as it was at onset, but this too produced mixed results. While warming at onset had mostly the expected effect of reducing height increases, the warming at breakdown had a more varied effect, seen in *figures 5.37 and 5.38*. Both adiabatic and advective terms are positive just before and just after block breakdown, contributing to the block lasting longer. While an increased height change effect was seen before the breakdown, after this time the effect was towards height falls, as seen in *figure 5.36*, depicting the total integrated height change.

CHAPTER 6

CONCLUSIONS

Multiple model runs using GFS Final Analysis and GFS Real-time forecast boundary conditions were used to diagnose the relevant conditions to block evolution, with specific attention to stratospheric thermal processes. Modifications were made to the real-time boundary conditions in an attempt to degrade the forecast from the good forecast that was made to potentially determine the factors most responsible for onset and breakdown of the 10-20 January 2009 blocking episode.

At onset, the warming of the cool areas had the biggest impact on weakening the block, potentially because it modified the widest area. The other warming modifications all had a similar impact, weakening the block at onset, but none of them delayed the onset or prohibited the block from forming. In these cases, the integrated adiabatic temperature change had the greatest impact on the overall thermally forced height change.

At breakdown the cooling of warm areas had the most noticeable impact in strengthening the block, again, based on the size of the area modified. In all modification cases for the breakdown the adiabatic temperature change dominated over the advective term, both in the stratosphere and troposphere. In the stratosphere during breakdown, however, the adiabatic and advective terms were positive and tended toward zero as the block decayed, whereas in the troposphere both terms were negative. So in the breakdown runs, both final analysis and modified, the stratosphere had an opposite effect as that in the troposphere.

The model appears to have had a corrective effect that had a greater impact than that due to the actual modifications. So any tweaking of the boundary con-

ditions reversed the effects taking place, either onset or decay. The greater of these impacts was on the decay of the block, as the modifications caused it to last longer than predicted, whereas at onset, the effect was to weaken the block without an changes to the timing of onset.

This partially satisfies the hypothesis that cooling in the stratosphere enhances blocking, and warming in the stratosphere is detrimental to blocking. While qualitatively this effect is seen in the differences between analyzed height and modified heights and in some integrated thermal processes, the modified model runs did not produce consistent quantitative results. Since the model seemed to correct for the modifications made, control was not able to be exerted over the temperature field at each particular time.

Further studies will need to be undertaken to ascertain the nature of boundary condition modification on a blocking event, with case studies on multiple blocking events rather than just a single event. Further modifications may also be done to additional parameters so that the height field matches the temperature field. An idealized study may also be undertaken to eliminate as many variables as possible, with more theoretical work to accompany it.

APPENDIX A

FORTRAN FUNCTIONS

Table A.1: Fortran Functions

Function Name	Description
stsb	Calculates static stability parameter, σ given θ, T, p, and a domain.
relax	Performs successive-over-relaxation of a function on given domain
FV	Calculates the vorticity forced height tendency forcing function on a given domain.
FT	Calculates the thermally forced height tendency forcing function on a given domain.
qgpv	Calculates quasigeostrophic potential vorticity given z, T, θ, p, σ, and a domain.
adv	Calculates the geostrophic temperature advection given z, T, p, and a domain.
intadia	Integrates adiabatic temperature change given ω, σ, p, a domain, and top and bottom pressure levels
intstrat	Integrates a field (either temperature advection or total temperature change) given the field, p, and a domain.
mxloc	Determines the location of maximum (in absolute value) of a given field

APPENDIX B

METEOROLOGICAL TERMS

Thermodynamics terms

Adiabatic: Heating or cooling as a result of a change in pressure without heat transfer.

Advective: Heating or cooling as a result of wind blowing across a temperature field. Horizontal advection is defined mathematically as $-\vec{V_H} \cdot \nabla_H T$ where V_H is horizontal wind and T is temperature

Diabatic: Heating or cooling as a result of processes other than adiabatic or advective, including radiation and latent heat.

Potential Temperature: The potential temperature θ is the temperature that a parcel of air at pressure p would have, if it were adiabatically brought to a reference pressure, p_0. Here $p_0 = 1000hPa$. θ is defined by the equation

$$\theta = T\left(\frac{p_0}{p}\right)^{\frac{R}{c_p}} \tag{B.1}$$

Dynamics Terms

Vorticity: A measure of rotation in a fluid flow, defined as the curl of the wind velocity vector $\zeta = \nabla \times \vec{V}$

Geostrophic: A balance between Coriolis and pressure gradient forces.

Coriolis Force: Apparent force due to the rotating earth, defined as $f = -2\vec{\Omega} \times \vec{V}$ where $\vec{\Omega}$ is the angular velocity of the earth.

Pressure Gradient Force: Force created by differences in pressure within a fluid. Defined as the negative gradient of the pressure field p,$-\nabla p$.

Geostrophic Wind: Wind that satisfies the geostrophic assumption, written as $\vec{V}_g$.

Geostrophic Vorticity: Curl of the geostrophic wind, written as ζ_g.

APPENDIX C

LOCATION GRAPHICS

The following appendix illustrates the polygon used to modify temperatures within the block, and the locations of the fastest height changes used in averaging integrals and the height change modifications.

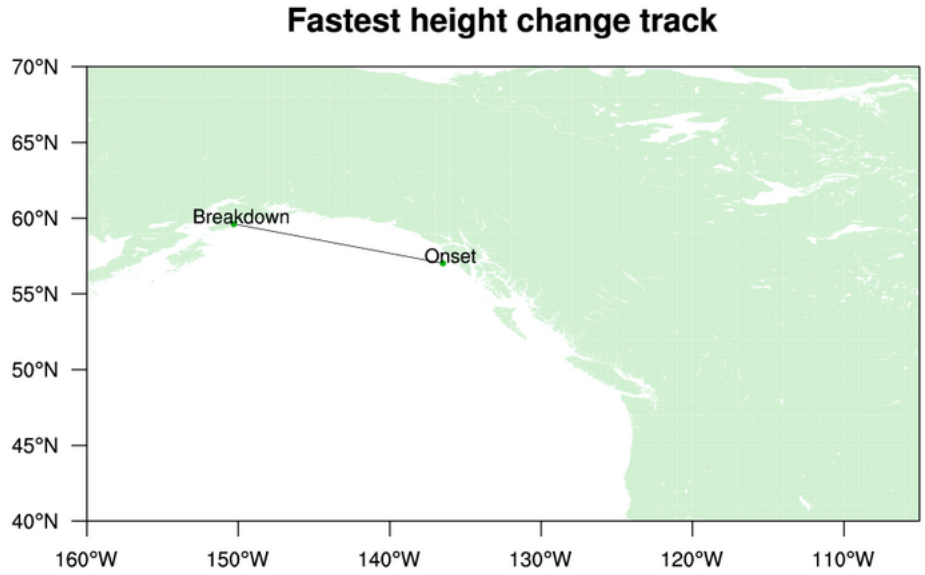

Figure C.1: Locations of fastest 12 hour height change in the time periods ending at onset and breakdown.

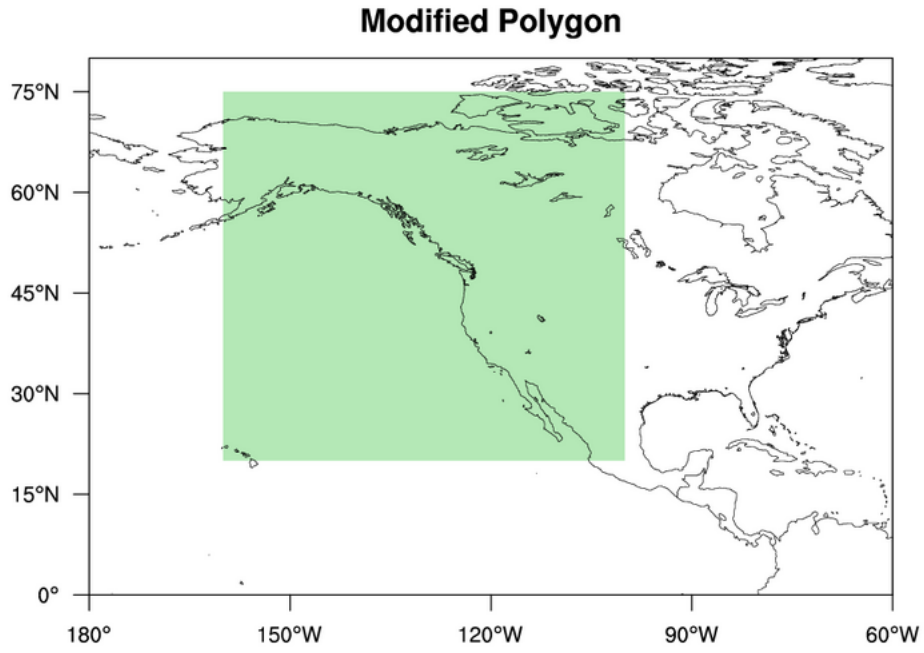

Figure C.2: Plot of modification polygon for ”in ridge” modifications.

BIBLIOGRAPHY

Carrera, M. L., R. W. Higgins, and V. E. Kousky, 2004: Downstream weather impacts associated with atmospheric blocking over the northeast pacific. *Journal of Climate*, **17**, 4823–4839.

Cash, B. A. and S. Lee, 2000: Dynamical processes of block evolution. *Journal of the Atmospheric Sciences*, **57**, 3202–3218.

Colucci, S. J., 2001: Planetary-scale preconditioning for the onset of blocking. *Journal of the Atmospheric Sciences*, **58**, 933–942.

— 2010: Stratospheric influences on tropospheric weather systems. *Journal of the Atmospheric Sciences*, **67**, 324–344.

Colucci, S. J. and T. L. Alberta, 1996: Planetary-scale climatology of explosive cyclogenesis and blocking. *Monthly Weather Review*, **124**, 2509–2520.

Dong, L. and S. J. Colucci, 2007: Interpreting the opposition between two block-onset forcing mechanisms. *Journal of the Atmospheric Sciences*, **64**, 2091–2104.

Garfinkel, C. I., D. L. Hartmann, and F. Sassi, 2010: Tropospheric precursors of anomalous northern hemisphere stratospheric polar vortices. *Journal of Climate*, **0**.

Holton, J. R., 2004: *An Introduction to Dynamic Meteorology*. Elsevier Academic Press, fourth edition.

Tilly, D. E., A. R. Lupo, C. J. Melick, and P. S. Market, 2008: Calculated height tendencies in two southern hemisphere blocking and cyclone events: The contribution of diabatic heating to block intensification. *Monthly Weather Review*, **136**, 3568–3578.

Trenberth, K. E. and C. J. Guillemot, 1996: Physical processes involved in the 1988 drought and 1993 floods in north america. *Journal of Climate*, **9**, 1288–1298.

UCAR, 2010: The weather research and forecasting model website. URL `http://wrf-model.org/`

Watson, J. S. and S. J. Colucci, 2002: Evaluation of ensemble predictions of blocking in the ncep global spectral model. *Monthly Weather Review*, **130**, 3008–3021.